

Truncation of the Binary Distribution Function in Globular Cluster Formation

E. Vesperini^{1,2} and David F. Chernoff²

¹ Scuola Normale Superiore,
Piazza dei Cavalieri 7, 56126-I, Pisa

² Department of Astronomy, Space Science Building, Cornell University,
14853 Ithaca (New York) USA

Abstract

We investigate a population of primordial binaries during the initial stage of evolution of a star cluster. For our calculations we assume that equal mass stars form rapidly in a tidally truncated gas cloud, that $\sim 10\%$ of the stars are in binaries and that the resulting star cluster undergoes an epoch of violent relaxation. We study the collisional interaction of the binaries and single stars, in particular, the ionization of the binaries and the energy exchange between binaries and single stars. We find that for large N systems ($N > 10^3$) even the most violent beginning leaves the binary distribution function largely intact. Hence, the binding energy originally tied up in the cloud's protostellar pairs is preserved during the relaxation process and the binaries are available to interact at later times within the virialized cluster.

Subject headings: clusters:globular, stars: binaries, stars: stellar dynamics

1 Introduction

Recent observational searches suggest that the frequency of primordial binaries in globular clusters may reach $\approx 10\%$ (see Hut et al. 1992 for a review). The inferred abundance of binaries is sufficiently large that both dynamical and collisional consequences are important. Several different treatments conclude that binaries are effective in halting core collapse, supporting the core and/or driving an expansion phase (Goodman & Hut 1989, McMillan et al. 1990, 1991, Gao et al. 1991, Heggie & Aarseth 1992). The abundance and binding energy distribution of the binaries have a direct impact on observable characteristics of globular clusters such as the size of the core radius (Vesperini & Chernoff 1994). The inferred abundance of binaries is consistent with that needed by stellar reaction pathways to account for the population of millisecond pulsars in the cluster system (Sigurdsson and Phinney 1994).

The fraction of binaries observed among field stars ($> 70\%$ see, e.g., Abt 1983, Duquennoy & Mayor 1991, and Reipurth & Zinnecker 1993 for the frequency of binary stars among pre-main sequence stars) is larger than the fraction, hitherto detected, in clusters. The size of the difference may be partially due to observational biases: binaries should segregate to the center of the cluster and may be difficult to find on account of stellar crowding. Or fewer binaries may have formed originally, some may be depleted by collisional effects and some visible members may be swapped by exchange reactions for heavy, degenerate and invisible remnants. Many lines of inquiry (reviewed by Hut et al. 1992) are being pursued to characterize the present binary content and binary binding energy distribution within clusters.

The key question we will address is whether it is possible for binaries, assumed to be primordial, to survive the birth of the cluster. The route for the formation of a bound cluster of stars is not well-understood but it is plausible that a hydrostatically supported gas cloud is a direct precursor to the stellar cluster. Such a cloud might form by cooling instability in the Galactic halo (Fall & Rees 1985) or in the cooling region behind a shock front after two gas clouds collide (MacLow & Shull 1986, Shapiro & Kang 1987). The narrowness of the main-sequence in Galactic globular clusters is

evidence that the epoch of star formation is brief. If star formation proceeds rapidly compared to the gravitational free-fall time, the resulting collection of stellar objects forms far out of virial equilibrium and a period of violent relaxation ensues. Stars exchange energy through fast, large-scale variation of the gravitational potential. Although the collapse is dissipationless, the gross properties (radius, velocity dispersion) of the system undergo damped oscillations until a virialized state is reached. During the intervals of high stellar density and high velocity dispersion collisional interactions occur with increased rate.

In this paper we will investigate the fate of a population of primordial binaries, paying particular attention to the process of disruption of binaries. Since the total binary binding energy can easily exceed the smooth, large-scale gravitational potential energy of the stars of the cluster, binary heating and softening are also potentially important processes to address. Although we treat only point-like stellar objects and assume all gas is removed at the conclusion of star formation, our conclusions have some applicability to the frequency of collisional interactions of stars with gaseous disks. Elsewhere, we will consider the implications for a scenario in which stellar disks are common once violent relaxation begins.

To address the issues, we explore the rate of collisional interactions between single stars and binaries. We determine how the binary distribution function is altered including the fraction of binaries destroyed and identify a characteristic binding energy below which the initial distribution is truncated. To anticipate our results to some extent, we find that collisional effects during the epoch of violent relaxation are small in the following sense: in the final, virialized state only *soft* binaries have been strongly effected (i.e. heated or ionized) when the number of stars N is as large as it typically is for a globular cluster. We explore the scaling of this conclusion with N .

The scheme of the paper is the following: in §2 we estimate the binary destruction that occurs during the violent relaxation; we discuss the rationale for carrying out an N-body experiment; in §3 we describe several tests of the N-body code designed to verify that it performs adequately in all regimes of interest; in §4 we describe the N-body runs and analyze the results; in §5 we

report a refined analytic estimate of the change in the binary distribution function. We are able to explain most of the significant trends in the N-body simulations and to verify the key role that ionization plays in the numerical experiment. In §6 we summarize the main conclusions and describe future work.

2 Violent relaxation and binary destruction: a simplified model

Let $\xi \equiv T/|V|$ be the initial ratio of kinetic to potential energy of the system. For the estimates in this section, we represent a stellar cluster by a uniform, spherically symmetric density distribution of radius R . If $\xi < 0.5$ the system collapses and oscillates with decreasing amplitude as it virializes. The first cycle of collapse and re-expansion (“bounce”) produces the densest central conditions. The bounce occurs when the kinetic energy associated with the particles’ dispersion becomes comparable to the potential energy. N -body calculations show that the discreteness may play a role in determining the cluster’s size at maximum collapse R_{mc} (Aarseth et al. 1988). If the initial velocity dispersion exceeds a given amount ($\xi \gtrsim N^{-1/3}$) then the minimum size scales like $R_{mc} \sim \xi R_i$. If the system is very cold, so that $\xi \lesssim N^{-1/3}$, and if the initial positions are randomly realized for a uniform density distribution then the discrete fluctuations induce a background of perturbations and $R_{mc} \sim N^{-1/3} R_i$.

If no star gains enough energy to escape and if the cluster remains homogeneous, then the virialized state satisfies energy conservation so that

$$-\frac{3}{5} \frac{GM^2}{R_i} (1 - \xi) = -\frac{3}{10} \frac{GM^2}{R_f} \quad (1)$$

where M and R_i are respectively the mass and the initial radius of the system. Hence, the final radius is

$$R_f = \frac{R_i}{2(1 - \xi)}. \quad (2)$$

If some of the stars escape from the system, changing the mass by $\Delta M = M_f - M_i$ and the energy by $\Delta E = E_f - E_i$ (where final values are indicated by “f”) but leaving the cluster homogeneous, then energy conservation implies

$$-\frac{3}{10} \frac{GM_f^2}{R_f} = -\frac{3}{5} \frac{GM_i^2}{R_i} (1 - \xi) + \Delta E. \quad (3)$$

The final radius is

$$R_f = \frac{R_i}{2(1 - \xi)} \frac{(1 + \Delta M/M_i)^2}{(1 + \Delta E/E_i)}. \quad (4)$$

If the system cools ($\Delta E < 0$) and/or loses mass ($\Delta M < 0$) then the final size is smaller than the case in which there is no change of energy; if the system heats ($\Delta E > 0$) but does not lose mass, the opposite is true.

For a system of single stars, van Albada (1982) showed that the magnitude of the mass and energy changes during violent relaxation is correlated to how cold the system is at the beginning. Small ξ implies violent, large amplitude oscillations in the cluster and large $|\Delta M|$ and $|\Delta E|$. When binaries are present and suffer collisional interactions within the cluster, the gain or loss of their binding energy is accompanied by changes in stellar translational energy.

The amount of energy tied up in the binary population can be substantial. Let the number of single stars, binary systems and total stars be N_s , N_b and $N = N_s + 2N_b$, respectively. The ratio of the binary internal binding energy to large-scale cluster binding energy ($3GN^2m^2/5R$) is $\alpha = (5f_b/6N)(R\langle 1/a \rangle)$, where $f_b = N_b/N$ is the fraction of binaries, m is the mass per star and $\langle 1/a \rangle$ is the cluster average of the inverse binary semi-major axis. For a tidally limited cluster, on a circular orbit of Galactocentric radius R_g with rotation velocity v_{rot} ,

$$\alpha = 114 f_b \left\langle \frac{\text{AU}}{a} \right\rangle \left(\frac{N}{10^5} \right)^{-2/3} \left(\frac{R_g}{10 \text{ kpc}} \frac{220 \text{ km/s}}{v_{rot}} \right)^{2/3} \left(\frac{m}{M_\odot} \right)^{1/3}. \quad (5)$$

For a newly formed cluster, the most uncertain element in the above estimate is probably $\langle 1/a \rangle$. The field binary distribution is peaked about a period $P \sim 10^{4.8}$ d; the period distribution $dN_b(P)/d \log P$ varies like a Gaussian

with $\sigma_{\log P} = 2.3$ (Duquennoy & Mayor 1991). The peak of the field star distribution corresponds to $a \sim 30$ AU but the quantity $\langle 1/a \rangle$ is effectively dominated by binaries of the smallest separation. For a cluster born with field-like binaries, taking a to be of order 30 AU and $f_b \sim 0.1$ (as observed today in globulars, rather than $f_b \sim 0.6$ as observed in the field, Duquennoy & Mayor 1991 and Reipurth & Zinnecker 1993) gives an ultra-conservative lower limit for α of 0.4. A more plausible estimate is that a extends to ~ 1 AU (as observed in the field population, and as required by millisecond pulsar production pathways that involve binary mass transfer), implying $\alpha \sim 11$.

For the available binding energy to play a dynamical role in the cluster evolution, binaries must interact collisionally. Collisional interactions occur most rapidly at the point of maximum contraction of the cluster when the background stellar density and velocity dispersion are largest. In the estimates here we will focus on ionization, however, our N -body treatment is completely general (§3 and 4) and includes all the point-like interactions of single stars and binaries. We characterize the binary destruction by the “cut-off” semi-major axis a_{cut} which corresponds to the smallest value of the initial semi-major axis a for which the probability of destruction is of order unity. Ionization in single encounters and cumulative energy changes by successive encounters both contribute to changes in the form of binary binding energy distribution and in the cluster’s translational energy.

The change in the number density of binaries (n_b) by ionizing collisions with single stars of density n_s is

$$\frac{dn_b}{dt} = -n_s n_b \langle \sigma v \rangle \quad (6)$$

where $\langle \sigma v \rangle$ is the rate coefficient, averaged over the relative velocity distribution. If the single stars and binaries both have Maxwellian velocity distributions, the rate coefficient may be written

$$\langle \sigma v \rangle = \pi a^2 V_{th} \mathcal{R}(x) \quad (7)$$

where $\mathcal{R}(x)$ is a function of the hardness factor $x \equiv \epsilon/mv_s^2$ (ϵ is the binary binding energy $Gm^2/2a$ and v_s is the single star, one-dimensional velocity

dispersion) given by fits to numerical simulations (Hut & Bahcall 1983) as

$$\mathcal{R}(x) = \frac{1.64}{(1 + 0.2A/x)(1 + \exp[x/A])}, \quad (8)$$

$V_{th} = 3(A/2)^{1/2}v_s$ is the dispersion in relative velocity and A is a constant. For the case of energy equipartition $A = 1$; for velocity equipartition $A = 4/3$. The process of violent relaxation leaves the stars in the cluster close to velocity equipartition.

Let the half-mass radius at the point of maximum contraction be $R_{h,mc}$. The density $\rho \sim MR_{h,mc}^{-3}$, the velocity $v_s \sim (GM/R_{h,mc})^{1/2}$ and the binary hardness $x \sim R_{h,mc}/aN$. The lapse of time spent by the system in its maximally contracted form is proportional to the dynamical time $t_{dyn,mc} \sim (G\rho_{mc})^{-1/2}$. The fractional decrease in binaries of size a is

$$\delta(a) \equiv \frac{1}{n_b} \frac{dn_b}{dt} t_{dyn,mc} \quad (9)$$

$$= C \left(\frac{a^2 N}{R_{h,mc}^2} \right) \mathcal{R} \left(B \left[\frac{R_{h,mc}}{aN} \right] \right) \quad (10)$$

where $C \simeq 1.16$ and $B \simeq 1.56$ are numerical coefficients obtained by keeping all the appropriate factors in the above estimates. If the binary is soft at the point of maximum collapse, then we have the following simple expression for the fractional decrease

$$\delta = 5.56 \frac{a}{R_{h,mc}}. \quad (11)$$

A more complete analysis is possible and is given in Appendix A. The cutoff semi-major axis (for which $\delta \sim 1$) is closely tied to the minimum scale of the collapse.

Aarseth et al. (1988) characterized the minimum scale for collapse of a cold spherical system without angular momentum. In basic agreement with their results our numerical work (in succeeding sections) shows that the system collapses to a minimum scale set by root-N fluctuations in the initial conditions. The theory predicts $R_{h,mc} \propto N^{-1/3}$ and we find

$$R_{h,mc} = \frac{R_{h,i}}{1.13N^{0.36}}. \quad (12)$$

For the homogeneous system of interest here, $R_i = 2^{1/3} R_{h,i}$, and

$$R_{h,mc} = \frac{R_i}{1.42N^{0.36}}$$

which implies

$$a_{cut} \sim 0.13 \frac{R_i}{N^{0.36}}. \quad (13)$$

The hardness of this binary, measured in the final virialized system, assuming no mass or energy loss during the epoch of violent relaxation, and making the approximation $\xi = 0$ is

$$x_{cut} \sim \frac{9.6}{N^{0.64}}. \quad (14)$$

If $N \gtrsim 10^2$ *only soft binaries are ionized*. The simple analysis indicates that violent relaxation truncates the binary distribution at a characteristic soft scale.

The estimates based on the simple model are potentially misleading because the model has the following shortcomings:

- (1) The model assumes homogeneity while numerical simulations (see, e.g., van Albada 1982, Aarseth et al. 1988) show that the collapse of an initially homogeneous cluster gives rise to a core-halo structure when the point of maximum contraction is reached and that strong density variations persist in the final state. Since the collisional reaction rates depend sensitively on density it is not clear how the estimates will be altered.
- (2) The rate coefficient for the model estimate of ionization is based on Maxwellian velocity distributions. Since there exist strongly ordered motions during the initial phase of violent relaxation, not thermal distributions, the rate of binary destruction may be inaccurate.
- (3) In a cold initial state, particles are correlated over long distances; bound binaries, triples, etc. are present in the initial conditions. The rate of destruction of these structures cannot be described with reaction rate coefficients for free particles impinging on a binary as assumed in the model.

N -body simulations are described in §3 and §4 which are free of these shortcomings. Qualitatively, they validate the conclusion of the simple model that only soft binaries are ionized. Quantitatively, they give a more accurate

description of the processes that are important in the evolution of the binary distribution function.

3 Tests of the numerical code used

Simulations have been carried out by a special N -body code designed for collisional problems (Jayaraman & Chernoff 1992). Forces are calculated using an oct tree and a low-order multipole expansion of the particles within a cell (following Salmon 1991). Particles have independent time steps; polynomial approximations are used to specify positions and velocities within given time-intervals. Updated polynomials are found using a predictor-corrector integration scheme with accuracy $O(\Delta t^{3.5})$. The tree's structure is exact with respect to current particle positions (i.e. it is not allowed to deform as in the treatment of McMillan and Aarseth 1993). The accuracy of the integration is controlled by two tolerance parameters, one for the integration step size (for both relative and absolute error controls) and one for the neighbor sphere size. Well-isolated, bound stellar pairs are treated in the following special manner. The internal degrees of freedom are regarded as unperturbed Kepler orbits and the pairs interact with the rest of the system as single entities having the total mass and momentum of the constituents. All non-isolated stellar pairs are treated as individual stars. The classification into isolated and non-isolated pairs is updated on each timestep. Close-encounters between singles and/or binaries are identified making use of the tree structure. When a close-encounter is detected the particles involved are advanced on a collision-based timescale, which is typically much shorter than the timestep a single star would take in a collisionless simulation. Since each object is advanced independently, the extra cost for handling close encounters in this way is not prohibitive. The code maintains collisionless equilibria including Plummer laws, King models and polytropes for many characteristic dynamical times.

Several simulations were designed to test critical aspects necessary for the simulations of interest. In the first set of tests the collapse of a homogeneous sphere of particles was followed. The evolution provides a good illustration

of the behavior of the system in the absence of primordial binaries and allows calibration of errors and comparison with previous results.

Table 1 summarizes the results of three runs with $N = 1000$. The stars are distributed homogeneously within a sphere with virial ratios $\xi = 0.25$, 0.1 and 0.01. The particle velocities are drawn from a flat 3d distribution function whose maximum value is determined by ξ .

The units of all runs have been chosen so that $G = 1$, the total initial mass of the system $M_i = 1$ and the initial radius of the system $R_i = 1$. The timescale for the homogeneous sphere to collapse is

$$t_{ff} = \sqrt{\frac{3\pi}{32G\rho_i}} = 1.11 \quad (15)$$

The system is already close to the state of virial equilibrium at $t = 1.3$; runs were stopped at $t = 2$. Figure 1 provides snapshots of the mass density profiles at $t = 0.5, 1.1, 1.5$, and 2 for the case $\xi = 0.01$. In agreement with van Albada (1982) the snapshots clearly show the development of a core-halo structure during the collapse. The central density reaches its maximum value at $t \simeq t_{ff}$ as expected.

Table 1 shows, in agreement with van Albada (1982; see his table [1]), the physical trends that clusters with smaller ξ have (i) a larger fraction of escaping stars, (ii) a greater energy change in the bound stars and (iii) a larger ratio of final to initial central densities, $\rho_{c,f}/\rho_{c,i}$. In agreement with the analytic model of §2 the final to initial half-mass radius, $R_{h,f}/R_{h,i}$ may be predicted from the observed mass and energy changes. Table 1 also gives an indication of the size of the numerical errors. For all runs herein, the numerical parameters have been adjusted to give relative energy errors $\lesssim 1\%$ over the entire course of the calculation.

The second test assesses the ability of the code to track collisional encounters not only during the phase of violent relaxation but also over relaxation-length timescales. The single and binary stars are homogeneously distributed in a sphere with $\xi = 0.01$ as above. Here $N = 1000$ with $N_s = 500$ and $N_b = 250$. The binaries have semi-major axis $a \simeq 9 \times 10^{-4}$ and zero eccentricity. In the virialized state, assuming no energy or mass loss, the binary's hardness is $x = 5/4Na \sim 1.4$.

The evolution of the system was followed well beyond the end of violent oscillations until $t = 8$ (approximately $\sim 7t_{ff}$). This corresponds to $\sim 100t_{dyn}$, where we employ the definition of Spitzer and Hart (1971)

$$t_{dyn} = \frac{1.58R_h^{3/2}}{M^{1/2}}, \quad (16)$$

evaluated in the virialized state. (Specifically, at $t = 2$, the measured value of the R_h implies $t_{dyn} \approx 0.07t_{ff}$.) The half-mass relaxation time $t_{rh} = Nt_{dyn}/26 \log(0.4N) \sim 15t_{dyn}$. The long period of quiescent evolution permits a significant number of binary-single interactions.

Figure 2 shows the energy budget of the stars within the systems split into four separate categories (analogous plots are shown in Heggie & Aarseth 1992) (i) into internal energy (i.e. negative binding energy of a binary) versus external energy (i.e. translational energy of a single star or of a binary center of mass plus large-scale potential energy) contributions and (ii) into retained (bound to the cluster) versus escaping particles. The separate quantities plotted are labeled E_{int} , $E_{int,esc}$, E_{ext} , and $E_{ext,esc}$. The total energy of the cluster is $E_{int} + E_{ext}$; the conserved energy is the sum of all four components.

Evolution proceeds through several distinct phases. *Infall* occurs for $t < t_{ff}$; there are no escaping particles yet. The binding energy associated with the binaries increases slightly (line of medium dashes) because the binaries are *hard* relative to the cold, background stellar distribution. The interactions that take place during this phase depend, in part, upon pre-existing bound configurations that have the opportunity to collapse and interact slightly before t_{ff} . The collisional interactions lead to a small degree of binary hardening and a concomitant heating of the stellar distribution, seen as a slight increase in the external energy (line of short dashes).

Mass *ejection* occurs near t_{ff} at the point of maximum contraction. This is the largest change that occurs over the course of the entire simulation. For the binary distribution realized, the external energy dominates the internal energy for the escaping matter, but this need not be true in general. The figure clearly indicates the corresponding decrease in the external energy of the matter that remains bound.

After the ejection has occurred, the binaries within the cluster *slowly evolve*. They soften (their internal binding energy decreases) while the external energy of the cluster decreases. There is little discernible mass or energy loss during this phase. (Note, no tidal field was imposed on the cluster.) Due to the ejection of mass and energy during the violent relaxation, the hardness of the binaries is ~ 0.4 , somewhat less than the value 1.4 anticipated on the basis of the homogeneous model. Since $x \lesssim 1$ the binaries soften.

The main check provided by this test is energy conservation: over the course of the entire run the relative energy conservation is $\sim 10^{-3}$.

4 *N*-body simulations

4.1 Gross Changes

In this section we describe a set of *N*-body simulations designed to answer the related questions: (1) Is cluster evolution grossly altered by the presence of the primordial binaries during the period of violent relaxation? (2) How is the binary distribution modified by collisional interactions? (3) Does significant mass segregation of the binary population occur? We take the initial stellar system to be spherical, homogeneous and cold ($\xi = 0.01$). We make these choices in an attempt to maximize the central density and the destruction and/or collisional interactions of the binaries. In another paper we will discuss the role of inhomogeneities induced by a tidal field in limiting the degree of compression.

The adopted units are $G = 1$, total initial mass is $M_i = 1$, initial radius $R_i = 1$. We first generate a set of initial conditions with single stars (mass m) and binaries composed of stars (of mass m) and refer to this as the “normal” case. For these runs, the initial binary fraction is $f_b = 0.05$ and all binaries begin with circular orbits. The distribution function for the binding energy ϵ is logarithmic, i.e. $dN = f(\epsilon)d\epsilon \propto d\epsilon/\epsilon$. The selected range of binary energies corresponds approximately to $x \in [0.13, 1.3]$ in a homogeneous, virialized state, assuming no energy or mass loss and encompasses the critical cutoff semi-major axis a_{cut} . All calculations are carried out to $t = 1.3$ at which

point the system is close to virial equilibrium. We also consider two variants of the normal case. In one variant, we swap a single star of mass $2m$ for each binary (“inert binaries”). In the other, we swap 2 unbound single stars for each binary (“all singles”). The suite of runs are summarized in Table 2.

Three pair-wise comparisons may be made. To assess the full effect of the presence or absence of binaries, we compare the normal run to the one with all singles. The difference depends on at least two physical effects present in the normal runs but absent in the runs with all singles: mass segregation of the binaries and collisional encounters between the binaries and the single stars. To gauge the effect of mass segregation alone we compare the runs with inert binaries to those with all singles. To judge the role of the binary internal degrees of freedom alone we compare inert binary runs to normal runs.

Our results shows that the presence of binaries has only a small influence on the overall dynamics. Table 3 compares some key quantities at $t = 1.3$ for runs. The relative differences in the total external energy of the bound particles, the half-mass radius of the bound particles and the mass of the bound particles are tabulated. Averages of these quantities are given when multiple realizations of the initial conditions were calculated. The first three sections of the table show that only small fractional differences have developed. Repeated realizations suggest that the differences are due to the random sampling of the initial conditions; in any case, no systematic differences between runs are observed.

The fourth section of Table 3 provides quantitative information on the mass segregation of actual and inert binaries. The final half mass radii of singles, inert binaries and real binaries are compared and some systematic trends emerge. In all runs with the inert binaries the heavy particles segregate compared to the singles. However, in most runs with real binaries the binaries are *less* concentrated than the singles, a consequence of the binary destruction and the collisional recoil that occurs most rapidly at the center. Clearly, the final spatial distribution of the binaries is as strongly influenced by the collisional encounters as by the process of mass segregation.

Table 4 examines changes in binary binding energy in the normal runs.

(Again average quantities are used where multiple realizations were calculated.) Although the *fractional* change in binary binding energy is sizeable, the magnitude of that change is small compared to the energy carried off by escaping particles. Taken together, the information in Tables 3 and 4 shows that the mass and energy losses from ejected particles dominate the changes caused by the presence of the binaries. The systematic influence of binaries is small compared to the intrinsic variations in escaping particles.

The maximum degree of contraction is a key factor influencing the rate of collisional interaction of the binaries. Table 5 gives the ratio of the initial half-mass radius $R_{h,i}$ to the half-mass radius at the time of maximum contraction $R_{h,mc}$ for the runs with different N . The best empirical fits to the degree of contraction are powerlaws in the total number of particles $N_* = N_s + N_b$.¹ Figure 3 displays $\log R_{h,i}/R_{h,mc}$ as a function of $\log N_*$ (mean values are used when multiple realizations were calculated). The best fit is

$$\frac{R_{h,i}}{R_{h,mc}} = 1.13N_*^{0.36}, \quad (17)$$

in good agreement with the analytical and numerical estimate of Aarseth et al. (1988) showing that $R_{h,i}/R_{h,mc} \propto N^{1/3}$.

From Tables 3, 4 and 5 we conclude (i) mass and energy loss is dominated by ejected particles, (ii) the final structure of the bound system is not grossly altered by the presence of binaries, (iii) the maximum compression during violent relaxation is not greatly altered by the presence of binaries. The particular choice of the form of $f(\epsilon)$ does not alter these conclusions as long as single-star binary interactions are more important than binary-binary interactions. For our goal of exploring the binary truncation process during violent relaxation, we are free to choose the form of $f(\epsilon)$ that best elucidates the truncation mechanism, as we do in the next section. We also conclude (iv) the spatial distribution of the binaries is sensitive to the physical effects of mass segregation and collisional interactions. Consequently, while (i)-(iii)

¹ We use N to indicate the total number of particles, $N = N_s + 2N_b$, and N_* to stand for the “effective” number of particles $N_* = N_s + N_b$. When we compare the results of section 2 to the N -body simulations we use the quantity N_* rather than N in the analytic formulae.

are independent of the particular choice of $f(\epsilon)$ that is not true for the final spatial distribution of binaries. For example, if $f(\epsilon)$ is dominated by high binding energy binaries, the system's evolution tends to the case of the inert binaries in which unambiguous mass segregation was evident.

The conclusions should not be significantly altered if ξ is changed. The initial conditions are very cold (small ξ), in the sense that discreteness rather than initial thermal dispersion governs the maximum compression during relaxation. The cold initial conditions make the epoch of relaxation particularly violent and maximize the collisional effects. If warmer initial conditions were used, particle ejection would decrease, total mass and energy losses would diminish and the binary internal energy changes would become relatively more important. As far as the collisional processes are concerned, warmer initial conditions give an early epoch that more closely resembles the quasi-stationary stage of evolution discussed in §3.

4.2 Ionization and hardening of the binary population

The changes to the number of binaries N_b and the binding energy distribution are the focus of this section. The initial conditions contain a range of binary binding energies $[\epsilon_{min}, \epsilon_{max}]$. At later times, a binary is taken to be any pair of particles with total binding energy exceeding ϵ_{min} .

Figure 4 shows the time evolution of $N_b(t)/N_b(0)$ for runs with varying total particle number $N = 1000$ (a), 2000 (b), 3000 (c) and 5000 (d). (Mean values are plotted for cases with multiple realizations.) Most of the destruction evidently occurs close to the instant the minimum radius is reached $1.1 < t < 1.2$. It also of interest that some binary destruction begins *before* that point. The runs with larger N suffer less of this early destruction.

Figure 5 shows the distribution of binding energies at the beginning (solid lines) and at the end of the simulation ($t = 1.3$, dashed lines) for the different values of N . It is quite evident that the softest binaries in the distribution suffer the greatest destruction. At the same time, it is also clear that some binary hardening occurs; in particular, all the final states include binaries with $\epsilon > \epsilon_{max}$.

Although all the binaries included in the above simulations have initially

circular orbits, none of our essential results are altered by considering a distribution of eccentricities. In fact, if ionization is mainly responsible for the observed destruction, as we will show below, no alteration is expected because the ionization rate depends very weakly on eccentricity (Hut & Bahcall 1983). As a test of this point we have carried out two additional simulations with $N = 1000$ (same initial virial ratio and binary fraction as the normal runs) but with all binaries having initially eccentric orbits ($e = 0.5$). In Figure 6 we compare the final distribution of binding energy of binaries from these runs with that resulting from simulations with binaries having initially circular orbits. No significant differences are evident.

Figure 7 shows the time evolution of the hardness x calculated using the numerically determined central velocity dispersion (the maximum value anywhere within the system.) The vertical extent of the line segment indicates the range of the hardness implied by the *initial* binary binding energy distribution. The figure shows that during the period before the phase of maximum contraction, the binaries are hard so, in a thermal distribution, one would expect them to harden, not disrupt. As a result, the early binary destruction (when hardening is expected) is noteworthy. Moreover, after the transition all the binaries are soft and, in a thermal distribution, would tend to become softer. As a result, the binary hardening observed at the end of the simulation for the largest initial binding energies is noteworthy.

The data on the hardening prompts a question: how does one explain the degree of hardening that is seen? Although the positions of single stars and binaries are randomly picked, the cold initial conditions guarantee that correlations between particles are “frozen in”; the system must evolve for $\sim t_{ff}$ before the rate of hardening can be calculated with the thermally averaged rate coefficients. In fact, the binary hardening inferred using thermally averaged rate coefficients (Heggie & Hut 1993) and the numerically determined density and velocity dispersion history is completely insufficient to explain the observed binary hardening *before* the period of maximum contraction or to explain the *total* binary hardening observed by the end of the simulation.

It appears that part of the explanation is that there exist bound triples present in the cold initial conditions. At $t = 0$ some binaries are bound

to their closest neighbor; the hardening of such bound systems cannot be described using the thermally averaged rate coefficients. To show that such systems are expected, consider replacing each binary with a single star with mass $2m$ located at the center of mass of the binary. Write the total energy of the system composed of the binary and the nearest neighbor:

$$E_{triple} = \frac{1}{2}\mu v^2 - \frac{Gm_1m_2}{d}, \quad (18)$$

where $m_1 = M_i/N$ is the mass of the single particle, $m_2 = 2m_1$ is the mass of the binary, $\mu = (2/3)m_1$ is the reduced mass of the system, $d = (4\pi/3)^{1/3}R_i/N^{1/3}$ is the initial average interparticle separation while $v^2 \simeq 1.2\xi GM_i/R_i$ is the initial mean velocity dispersion. We find

$$E_{triple} = \frac{GM_i^2}{R_i} \left(\frac{0.4\xi}{N} - \frac{1.24}{N^{5/3}} \right) \quad (19)$$

which for $\xi = 0.01$ and $N \sim 10^3$, as in our simulations, is negative. The triple begins near apocenter; if half the triple's period is less than t_{ff} , pericenter will be reached before the point of maximal contraction. If the minimum distance between the binary and the single is less than the semi-major axis of the binary, a strong interaction and binary hardening is a likely outcome. We estimate t_{triple} , half of orbital period of the single around the binary star, to be

$$t_{triple} \approx 2.1t_{ff}. \quad (20)$$

It is plausible that some binaries have a close interaction before t_{ff} and this is probably responsible for the hardening that takes place at early times. These encounters cannot cause ionization because the total energy of the triples is negative.

As check of the above arguments we have followed the binaries in the run with $N = 3000$. The number of binaries initially present in this run is $N_b = 150$; 70 are initially bound to the closest particle to form a triple system. The cumulative distribution function of the distance of the distance to this closest particle, d_{cp} , is shown in Figure 8a at three different times before maximum collapse ($t = 0, 0.5$ and $1.$). As expected, the distance contracts

as the system collapses. In Figure 8b all the values of d_{cp} at $t = 0.5$ and $t = 1.0$ have been rescaled by the factor $R_{h,i}/R_h(t)$. About 80% of the triples collapse more quickly than the system as a whole. This is roughly consistent with the cumulative distribution function of t_{triple} in Figure 8c showing that 60% of the triples initially present in the system have $t_{triple} < t_{ff}$. Thus, it appears that a sizable fraction of triple configurations have the time to collapse, i.e. to reach pericenter, before maximum contraction.

Figure 8d shows the cumulative distribution function of the ratio of the semimajor axis of the binary, a , to the pericenter of the weakly bound element of the triple, p . Nine binaries satisfy $p < 2a$ and $t_{triple} < t_{ff}$, conditions which guarantee a strong interaction. This supports the hypothesis that *some* hardening occurs because of the interaction of singles and binaries initially bound in triple systems and that the hardening can occur before the bounce.

It is important to note that a triple is not necessarily destroyed at $t \sim t_{ff}$. Hierarchical triples with $p \lesssim 2.75 - 3.5a$ (Harrington 1972) are inherently unstable and, left alone, will eventually interact. The loosely bound outer star is expected to harden the binary when the interaction occurs. Also, if the triple encounters a single star it may produce an interaction with the binary member. It is possible, but unproven, that nearly all the triples will suffer strong interactions.

When triples are abundant the initial configuration may be more important for binary hardening than subsequent thermal single-star binary encounters. For a hard binary, the number of single-star binary encounters with a minimum distance of separation $\lesssim a$ over the course of the period of violent relaxation is $\sim N_b a / R_{h,mc}$ where N_b is the total number of binaries. Since $R_{h,mc} \sim R/N^{1/3}$ and since the binary binding energies in the numerical runs have been scaled so as to keep x in the final virialized state fixed, $a \propto R/N$, it follows that the number of binary-single encounters in the N-body calculations $\sim N_b / N^{2/3}$. Let N_3 be the number of bound triples that ultimately give a strong binary interaction. The ratio of triple encounters to single-star binary encounters scales like $N_3 N^{2/3} / N_b$; if the system is so cold that each binary is bound in a triple (eqn. [19]) and if each triple suffers a strong

interaction, then the ratio increases with N . In fact, the observed change in binding energy increases with N in the set of simulations.

In summary, the cold initial conditions include bound triples (and possibly higher-order assemblies) that interact and produce hardening in some binaries before the point of maximum contraction is reached. Bound triples may dominate the hardening after a free-fall time.

4.3 Cutoff binary binding energy

We now investigate the quantitative determination of the cutoff binary semi-major axis a_{cut} , or equivalently, the cutoff binding energy ϵ_{cut} . We first introduce an *empirical* determination based on comparison of the initial and final cumulative distribution function (CDF) of the binding energy. Figure 9 gives the CDFs (initial and final) normalized by the initial total number of binaries. We define the cutoff to be the crossover point between the two curves. This definition of the cutoff is not the same that we have used in §2 or §5 so we discuss its plausibility.

The cross over point identifies the value of the binding energy ϵ_{cut} such that the total number of more tightly bound binaries is the same as in the initial conditions ($\Delta N = N_f(> \epsilon) - N_i(> \epsilon) = 0$). *If* it were true that ionization was the only process responsible for modifying the binary binding energy distribution, this definition would not be very useful because some destruction can occur at all energies so $\Delta N < 0$ for all ϵ . A more meaningful definition might involve a significant relative change ($\Delta N/N_i(> \epsilon) = \text{const}$).

On the other hand, it is clear from the CDFs in Figure 9 that ionization is *not* the only process modifying the properties of the binary star population. Significant hardening occurs for large ϵ (evident from the fact that the final CDF is much larger than the initial CDF for $\epsilon > \epsilon_{cut}$). This hardening, which we have discussed in the previous section, is caused in part by the bound triples in the initial configuration. Such encounters do not lead to ionization and the rate of hardening encounters does not appear to be very sensitive to ϵ . For soft binaries the rate of thermal ionization scales like a (and Figure 7 shows that $x < 1$ at the cluster center) so it is clear that ionization is most effective at small binding energies. Hence, the numerically determined

crossover point occurs at a point where the rate of ionizing encounters exceeds the rate of hardening encounters.

The numerical results are well fit by the following expression

$$\epsilon_{cut} = \frac{1.14}{N_*^{1.19}} \frac{GM_i^2}{R_i}. \quad (21)$$

Since $a = GM_i^2/(2N^2\epsilon)$, it follows

$$a_{cut} = \frac{0.40}{N_*^{0.81}} R_i. \quad (22)$$

This numerical result differs in two ways from the theoretical estimate (based on the simple model in §2) which gave

$$a_{cut} = \frac{0.13}{N^{0.36}} R_i. \quad (23)$$

The ratio of the two results is $\sim 0.33N^{0.45}$; for $N = 1000$ the ratio is about 7, for $N = 5000$ about 15. That the magnitudes differ by such factors is understandable given the variety of approximations of the simple model. The difference in scaling is, however, more of a puzzle.

There appear to be two possible explanations and they are not mutually exclusive. First, in the analytic estimate, the asymptotic form for the ionization rate $\mathcal{R}(x)$ for a soft binary was used. As the system evolves, a binary goes from being hard to soft and the relevant asymptotic description for $\mathcal{R}(x)$ changes. Details may be found in Appendix A. Second, from the discussion of the initial correlations of the cold system, it is clear that the frequency of occurrence and the binding energy of the triples both depend upon N . Only if $N \gg 10^3$ is the nearest star likely to be unbound to the binary. It is not easy to perform an a priori estimate of the scaling when such effects are present. Given these uncertainties (in addition to those connected with the original definition of the cutoff) we also provide a more detailed calculation of the change in the full binary distribution function in the next section.

The 1-dimensional mean square velocity dispersion in the virialized cluster is

$$v_f^2 \simeq \frac{2}{15} \frac{GM_f}{R_{h,f}} \quad (24)$$

derived by means of the virial theorem and taking the total energy of the system equal to $|E| = GM_f^2/(5R_{h,f})$ (see, e.g., Binney & Tremaine 1987) where M_f is the final cluster mass and $R_{h,f}$ is the final half-mass radius. The hardness of the cutoff binary is

$$x_{cut} = \frac{\epsilon_{cut}}{mv_f^2} = 3.75 \frac{R_{h,f}}{a_{cut}N} \frac{M_i}{M_f}. \quad (25)$$

and the scaling of x_{cut} with N depends not only on the variation of ϵ_{cut} but also on the mass and energy ejection from the system. The values of x_{cut} for the simulations done are [0.445, 0.342, 0.257, 0.154] for $N = 1000, 2000, 3000,$ and 5000 , respectively. Assume (i) that M_f and $R_{h,f}$ are well-determined. Table 5 shows that the mass and energy loss do not vary greatly over the entire set of runs. And, (ii) that the analytic scaling for a_{cut} governs for $N > 5000$. Then, the best empirical fit for the cutoff hardness is

$$x_{cut} = \frac{43}{N^{0.65}}. \quad (26)$$

Clearly, as N increases, x_{cut} decreases. For all cases investigated, the binaries destroyed in the course of the collapse are unimportant in terms of the energetics of the cluster and do not modify the dynamics of the collapse nor the final state resulting from it.

5 Analytical estimate of the effects of ionization on the binary stars

We begin with an estimate of how the binary distribution function evolves if thermal ionization were the only operative process and if no mass segregation occurred.

We tabulated the time evolution (from $t = 0$ to $t = 1.3$) of number density, $n_s(t)$, and velocity dispersion, $v_s(t)$, of single particles at a set of 11 Lagrangian mass radii, r_M , from the N-body calculations. We assumed the binaries to be associated with fixed Lagrangian radii throughout the simulation. Using the ionization rate (6) we calculate $P(\epsilon, r_M)$, the probability

of destruction for a binary of energy ϵ at r_M . Figure 10 shows the function $P(\epsilon, r_M)$ for the runs with $N = 1000$. The largest ionization probabilities for each value of binding energy are, as expected, those calculated at the innermost Lagrangian radii where n_s and v_s reach the highest values.

The final binding energy distribution may be approximated

$$f(\epsilon, t = 1.3) = f(\epsilon, t = 0)[1 - \delta(\epsilon)] \quad (27)$$

where

$$\delta(\epsilon) = \frac{\int P(\epsilon, r)n_b d^3r}{\int n_b d^3r}. \quad (28)$$

Figure 11 shows the initial and the final distribution function for runs with $N = 1000, 2000, 3000$ and 5000 (dots give the final binding energy distribution function for the N -body simulation, the dashed line gives the initial distribution and the solid line gives the above estimate of the final distribution). The binary hardening at the largest values of ϵ is evident from the points that lie to the right of the initial range of the distribution. Apart from this effect, the agreement between the two calculations is satisfactory. Thermal ionization is responsible for the large changes that occur at low energies.

Next, we account for the effect of the triple configurations. Figure 12 shows the initial and final CDF for the run with $N = 3000$ from N -body data (solid lines) and the analytic estimate (dashed line). For small values of binding energy ($\epsilon/m_*\sigma^2 < 11$) the analytic CDF is determined by thermal ionization, as above. The agreement is good for binaries less bound than the crossover point. For higher values of the binding energy we assume that each binary undergoes a single hardening encounter with a mean change of $\Delta\epsilon = 0.4\epsilon$ (Heggie 1975). The resultant final CDF agrees well with the numerical CDF.

Finally, we compare the calculation of ϵ_{cut} and the total fraction of binaries ionized with the results of the N -body simulations (Tables 6 and 7). To find ϵ_{cut} , we've chosen $\delta = 0.21$ so that the crossover point of the analytic and numerical results agree in the run with $N = 1000$. (Any value of δ of order 1 is *a priori* reasonable.) The cutoff energy and the fraction of ionized binaries

both follow in the analytic model, once this choice has been made. Values are compared with the values obtained directly from N-body simulations in §2. The agreement is quite good and suggests that the cutoff energy and binary ionization is controlled by thermally averaged ionization.

6 Conclusions and Future Work

We have investigated how a population of primordial binaries is modified by an epoch of violent relaxation. We have mostly focused on very cold initial conditions because they give rise to the maximum degree of contraction and, hence, the strongest collisional effects. We have used a binary fraction $f_b = 0.05$, thought to be typical of today's globular clusters.

With a combination of analytic and N-body calculations we find the following:

1. There is no significant change in the gross cluster properties at the end of violent relaxation due to the interaction between internal (binary) degrees of freedom and translational degrees of freedom.
2. There is a characteristic binding energy ϵ_{cut} such that binaries with $\epsilon > \epsilon_{cut}$ are not significantly disrupted, while for $\epsilon < \epsilon_{cut}$, ionization is the main destructive process.
3. The truncation in the energy distribution of the binary population occurs for hardness parameter $x < 1$, as calculated in the virialized system.
4. As the number of particles N increases, collisional effects become less important and the cutoff binding energy decreases.
5. The rate of hardening of binaries with $\epsilon > \epsilon_{cut}$ observed in the N -body simulations is not described by the thermally averaged rate coefficients. Cold initial conditions used for the simulations mean some binaries are bound to the closest single particle. An interaction between the single

particle and the binary is responsible for at least part of the observed hardening.

The scaling of the cutoff energy and the cutoff semi-major axis with the number of particles in the system may be related to the size of the system at the moment of maximum contraction. Reasonable agreement between N -body simulations and analytic estimates is found.

Future work may attempt to increase the fraction of binaries, to incorporate a spectrum of masses, to include gas, and to consider inhomogeneous initial conditions.

Acknowledgements

We thank the referee Sverre Aarseth for his comments that led us to extend and improve the manuscript. D.F.C. acknowledges grants NAGW-2224; E.V. acknowledges financial support from Scuola Normale Superiore and the hospitality of the Department of Astronomy of Cornell University.

References

- Aarseth S.J., Lin D.N.C., Papaloizou J.C.B., 1988, ApJ, 324, 288
Abt H.A., 1983, ARAA, 21, 343
Binney J., Tremaine, S. 1987, Galactic Dynamics (Princeton: Princeton Univ. Press)
Duquennoy A., Mayor M., 1991, A&A, 248, 485
Fall M.S., Rees M.J, 1985, ApJ, 298, 18
Gao B., Goodman J., Cohn H., Murphy B., 1991, ApJ, 370, 567
Goodman J., Hut P., 1989, Nature, 339, 40
Harrington R.S., 1972, Celest. Mech., 6, 322
Heggie D.C., 1975, MNRAS, 173, 729
Heggie D.C., Aarseth S.J., 1992, MNRAS, 257, 513
Heggie D.C., Hut, P. 1993, ApJS, 85, 347
Hut P., 1983, 268, 342
Hut P., Bahcall J.N., 1983, ApJ, 268, 319
Hut P., McMillan S.L.W., Goodman J., Mateo M., Phinney E.S., Pryor C., Richer H.B., Verbunt F., Weinberg M., 1992, PASP, 104, 981
Jayaraman S., Chernoff D.F., 1992, unpublished report
MacLow M., Shull J.M., 1986, ApJ, 302, 585
McMillan S.L.W., Aarseth S., 1993, ApJ, 414, 200
McMillan S.L.W., Hut P., Makino J., 1990, ApJ, 362, 522
McMillan S.L.W., Hut P., Makino J., 1991, ApJ, 372, 111
Reipurth B., Zinnecker H., 1993, A&A, 278, 81
Salmon, J.K. 1991, Ph.D. Thesis at Cal Tech
Shapiro P.R., Kang H., 1987, ApJ, 318, 32
Sigurdsson S., Phinney E.S. 1994, preprint
Spitzer L., Hart M.H. 1971, ApJ, 164, 399
van Albada T.S., 1982, MNRAS, 201, 939
Vesperini E., Chernoff D.F., 1994, ApJ, 431, 231

Appendix A

In deriving expression (11) for $\delta(a)$ we have assumed that the cut-off binding energy falls in the very soft regime at the moment of maximum collapse of the system; the scaling law (13) for a_{cut} that follows from eq.(11) is different from that obtained from N -body simulations. An explanation may be due in part to the fact that if the cut-off binding energy does not fall in the very soft regime at the moment of maximum contraction, as we have assumed above, the approximate expression for $\mathcal{R}(x)$ we have used is incorrect. In the following we will show that depending on the hardness factor of the cut-off binding energy at the moment of maximum contraction three different scaling laws for a_{cut} hold. If we define

$$\tilde{a} \equiv a/R_{h,mc} \quad (29)$$

we can write

$$\delta(a) = C\tilde{a}^2 N \mathcal{R}(B/[\tilde{a}N]) \quad (30)$$

where B and C are numerical constants introduced in the text.

It is easy to show that for some range of values of $\tilde{a}N$,

$$\delta(a) = \begin{cases} 5.56\tilde{a}, & \text{if } \tilde{a}N \rightarrow \infty, \\ 0.47\tilde{a}^2 N, & \text{if } \tilde{a}N \sim B, \\ 1.9\tilde{a}^2 N e^{-B/\tilde{a}N}, & \text{if } \tilde{a}N \rightarrow 0 \end{cases} \quad (31)$$

Thus it is clear from the above considerations that, in relation to the spacing between the solutions of the equation $\delta(a) = \text{const.}$ used to define the cut-off binding energy (or semi-major axis) there exists three different regimes:

1. $N \rightarrow \infty$: δ enters the linear regime for very small values of \tilde{a} and does not depend on N so that $\tilde{a}_{cut} = \text{const.}$
2. 'Intermediate' N : solutions in the regime where $\delta(a) \sim \tilde{a}^2 N$ and thus $\tilde{a}_{cut} \sim N^{-1/2}$.
3. Low N : a steeper decrease with N than $\tilde{a}_{cut} \sim N^{-1/2}$ is expected.

The N -body calculations, described in the text, with $N \sim 10^3 - 10^4$ have a scaling for \tilde{a} that is close to the 'intermediate' N regime ($\tilde{a} \propto N^{-0.45}$ in this range). If, in calculating the solution of $\delta(a) = \text{const.}$, we choose the value of the constant ($\simeq 0.003$) so to get the correct scaling for the range of N investigated, we obtain the following estimates for a_{cut}

$$a_{cut} = \begin{cases} 0.19R_{h,mc}N^{-0.65}, & \text{for } N < 500 \\ 0.08R_{h,mc}N^{-1/2} & \text{for } 500 < N < 2000, \\ 5.39 \times 10^{-4}R_{h,mc}, & \text{for } N \rightarrow \infty \end{cases} \quad (32)$$

For the range of N spanned by numerical simulations ($950 < N_* < 4750$) the curve of the solutions of the equation $\delta(a) = \text{const.}$ is well fitted by

$$a_{cut} = \frac{0.05}{N_*^{0.44}}R_{h,mc} \quad \text{for } 950 < N_* < 4750 \quad (33)$$

In this way we can obtain the observed scaling but there are still two difficulties: 1) in order to get the correct scaling in the range of N where it is observed in N -body simulations we have been forced to choose a value of the constant that is very small and it is not clear why such a small value should be connected with the cut-off energy; 2) the numerical constant in eq.(33) is much smaller than the value found from N -body simulations. The latter point is likely to be due, at least in part, to the very approximate estimates for the density and velocity dispersion used to calculate $\delta(a)$ and for this reason a more accurate analytical estimate has been carried out in §5 of the paper.

Figure Captions

Figure 1 Mass density profiles for the run with $N = 1000$ and initial virial ratio $T/|V| = 0.01$ (no binaries) at (a) $t = 0.5$, (b) $t = 1.13$, (c) $t = 1.3$ and (d) $t = 2$.

Figure 2 Energy budget for the test run with $N_s = 500$ single particles and $N_b = 250$ binaries. Total external energy of bound particles (short dashed line), total external energy of escaping particles (solid line), total (internal) binding energy of binaries bound to the system (dashed line) total (internal binding) of escaping binaries (long dashed line) (see text for definitions). Note that the internal binding energy of the binaries is taken here with negative sign.

Figure 3 Ratio of the initial half-mass radius to the half-mass radius at the time of maximum contraction. The dashed line is the best-fit line and it is proportional to $N_*^{0.36}$.

Figure 4a-d Time evolution of the number of binaries normalized to the initial number of binaries. For the values of N (1000, 2000) for which two simulations have been carried out the mean value and the semidispersion as error bar are plotted. a) $N = 1000$; b) $N = 2000$; c) $N = 3000$; d) $N = 5000$

Figure 5a-d Histograms of the binding energy at the beginning of simulation (solid line) and at the end of the simulation (dashed line) (a) $N = 1000$; (b) $N = 2000$; (c) $N = 3000$; (d) $N = 5000$.

Figure 6 Histograms of the binding energy at the end of the simulations with $N = 1000$ and binaries initially with circular orbits ($e = 0$) (solid line) and eccentric orbits ($e = 0.5$) (dashed line). Dots have been put on the histogram corresponding to the runs with binaries with initial eccentricity $e = 0.5$ to distinguish the two curves where they overlap.

Figure 7a-d Time evolution of the hardness factor x calculated at the center of the system (see text for the definition) for the range of values of binding energy put in the initial conditions of N-body simulations. The upper and the lower point of each bar are the hardness factor of the upper and lower values of binding energy initially put in the systems (a) $N = 1000$; (b) $N = 2000$; (c) $N = 3000$; (d) $N = 5000$.

Figure 8a-d (a) Cumulative distribution function of the distance, d_{cp} , between the closest particle and the binary forming bound triple systems at $t = 0$ (solid line), at $t = 0.5$ (short dashed line) and at $t = 1$ (long dashed line); (b) as 10a but with the distances d_{cp} at $t = 0.5$ and $t = 1$ rescaled by a factor $R_{h,i}/R_h(t)$; (c) Cumulative distribution function of t_{triple} (see text); (d) Cumulative distribution function of the ratio of the semimajor axes of the binaries bound in triple systems to the pericenter distances between the binaries and the singles in the triple systems at $t = 0$. All the data refers to the run with $N = 3000$.

Figure 9a-d Initial (solid lines) and final (dashed lines) cumulative distribution functions of the binding energy of binaries in the N-body simulations normalized to the initial number of binaries. (a) $N = 1000$; (b) $N = 2000$; (c) $N = 3000$; (d) $N = 5000$.

Figure 10 Destruction probability $P(r_M, \epsilon)$ as function of binding energy and Lagrangian radius (see text for the analytical derivation)

Figure 11a-d Final binding energy distribution function from N -body simulations compared with the final binding energy distribution function derived analytically (solid lines). Dashed lines show the initial binding energy distribution function. (a) $N = 1000$; (b) $N = 2000$; (c) $N = 3000$; (d) $N = 5000$.

Figure 12 Initial and final cumulative distribution function from N-body simulation (solid lines) for the run with $N = 3000$ and the final cumulative distribution function from analytical estimates (dashed line) calculated as described in the text: 1) $\epsilon/m_*\sigma^2 < 11$ ionization only; 2) $\epsilon/m_*\sigma^2 > 11$ hardening: initial energy shifted by an amount equal to the mean change in energy per encounter $\sim 0.4\epsilon$.

Table 1
Summary of test results

ξ	E_i	E_f	$\Delta M/M_i$	$\rho_{c,f}/\rho_{c,i}$	$R_{h,f}/R_{h,i}$	$ \Delta E/E_i $
0.25	0.44	0.44	-	19.4	0.45	5×10^{-4}
0.1	0.53	0.61	0.15	115.6	0.26	3×10^{-4}
0.01	0.59	0.92	0.18	1227	0.17	2×10^{-4}

Table 1: Summary of test results. All runs have $M_i = 1$, $R_i = 1$ and $N = 1000$. The final time is $t = 2$, ξ is the initial virial ratio $T/|V|$, E_i is the total initial energy, E_f is the total final energy of particles bound to the system, $\Delta M/M_i$ is the fractional mass loss, $\rho_{c,f}/\rho_{c,i}$ is the ratio of final to initial central densities, $R_{h,f}/R_{h,i}$ is the ratio of final to initial half-mass radii, and $\Delta E/E_i$ is the fractional change in energy due to computational errors.

Table 2
Initial conditions for N-body

N	# runs			$\epsilon/m\sigma^2$	$\epsilon/m_*\sigma^2$	eccentricity
	Normal	Inert Binaries	Singles			
1000	2	2	2	5-50	5-50	0
1000	2	0	0	5-50	5-50	0.5
2000	2	2	2	5-52	2.5-26	0
3000	1	1	1	5-60	1.66-20	0
5000	1	1	1	5-60	1-12	0

Table 2: Initial conditions for the N-body simulations. All runs have $M_i = 1$, $R_i = 1$ and an initial virial ratio $\xi = 0.01$. N is the number of stars. Normal runs include $0.9N$ singles and $0.05N$ binaries, inert binary runs include $0.9N$ singles and $0.05N$ singles (of mass $2m$), and single runs include N singles. For runs with binaries, the range of binding energies is given $\epsilon/m\sigma^2$ (and $\epsilon/m_*\sigma^2$), where m is mass per particle and $m_* = 10^{-3}$, and $\sigma = \sqrt{\xi \frac{GM_i}{R_i}}$ is proportional to the initial velocity dispersion.

Table 3
Comparisons

N	$\frac{\Delta E_{f,b-s}}{E_{f,b}}$	$\frac{\Delta E_{f,b-ib}}{E_{f,b}}$	$\frac{\Delta E_{f,ib-s}}{E_{f,ib}}$
1000	0.029	0.099	-0.077
2000	0.012	-0.087	0.091
3000	0.043	0.081	-0.041
5000	0.014	0.139	-0.145
N	$\frac{\Delta R_{h,b-s}}{R_{h,b}}$	$\frac{\Delta R_{h,b-ib}}{R_{h,b}}$	$\frac{\Delta R_{h,ib-s}}{R_{h,ib}}$
1000	-0.043	-0.064	0.020
2000	0.093	0.225	-0.170
3000	0.112	-0.041	0.147
5000	-0.003	-0.153	0.132
N	$\frac{\Delta M_{f,b-s}}{M_{f,b}}$	$\frac{\Delta M_{f,b-i}}{M_{f,b}}$	$\frac{\Delta M_{f,ib-s}}{M_{f,ib}}$
1000	-0.004	-0.019	0.015
2000	0.005	0.036	-0.032
3000	0.035	0.001	0.034
5000	-0.014	-0.012	-0.002
N	$\frac{(R_{h,f}(s)-R_{h,f}(ib))}{R_{h,f}(s)}$	$\frac{(R_{h,f}(s)-R_{h,f}(b))}{R_{h,f}(s)}$	
1000	0.17	-0.15	
2000	0.23	-0.38	
3000	0.16	-0.11	
5000	0.13	0.02	

Table 3: The first three sections report fractional differences in the final energy (ΔE_f), half-mass radius (ΔR_h) and mass (ΔM_f) for particles remaining bound to the cluster at $t = 1.3$. The parameters of the runs are listed in Table 2. Each column applies to a pair of runs identical except for their treatment of the binary component. The pairs are identified by the subscripts “b”, “s”, “ib” which refer to runs with normal binaries, with all singles and with inert binaries respectively.

The fourth section reports the fractional differences in the half mass radii of separate components in the same run. $R_{h,f}(s) - R_{h,f}(ib)$ is the difference between the final half-mass radius of singles and inert binaries in the runs with inert binaries. $R_{h,f}(s) - R_{h,f}(b)$ is the difference between the final half-mass radius of singles and binaries in the runs with normal binaries.

Table 4
Changes in binding energy

N	$\frac{\Delta E_B}{E_{esc}}$	$\frac{\Delta E_B}{E_{B,i}}$
1000	-0.006	-0.23
2000	-0.007	-0.29
3000	0.0	-0.02
5000	0.005	0.39

Table 4: A comparison of average relative energy changes for particles bound to the cluster at $t = 1.3$ for runs with normal binaries. ΔE_B is the difference between final and initial internal energy (negative binding energy) of binaries bound to the cluster, E_{esc} is the total external energy carried away by escaping particles, and $E_{B,i}$ is the total initial binary binding energy.

Table 5

N	type	$R_{h,i}/R_{h,mc}$	$ \Delta M /M_i$	$ \Delta E /E_i$
1000	Singles	13.4	0.20	0.71
		12.3	0.19	0.60
	Inert binaries	11.0	0.20	0.53
		11.6	0.17	0.56
	Normal	13.7	0.22	0.79
2000	Singles	13.7	0.17	0.63
		13.1	0.21	0.68
	Inert binaries	14.7	0.22	0.93
		17.3	0.23	0.99
	Normal	15.3	0.25	0.95
3000	Singles	14.8	0.21	0.82
		14.7	0.21	0.83
	Inert binaries	16.7	0.25	1.07
		17.2	0.23	1.00
	Normal	19.1	0.23	1.17
5000	Singles	18.4	0.24	1.20
	Inert binaries	18.4	0.27	1.15
	Normal	23.8	0.28	1.51

Table 5: The degree of compression, mass loss and energy change in the N-body simulations. $R_{h,i}/R_{h,mc}$ is the maximum ratio of initial to half-mass radii over the course of the calculation. ΔM is the difference between the final and the initial mass and ΔE is the difference between the final and the initial external energy of the particles bound to the system.

Table 6

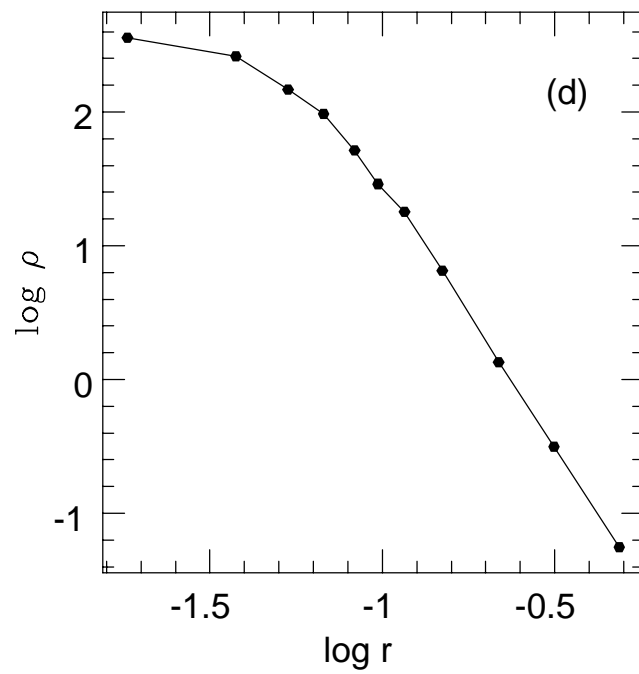
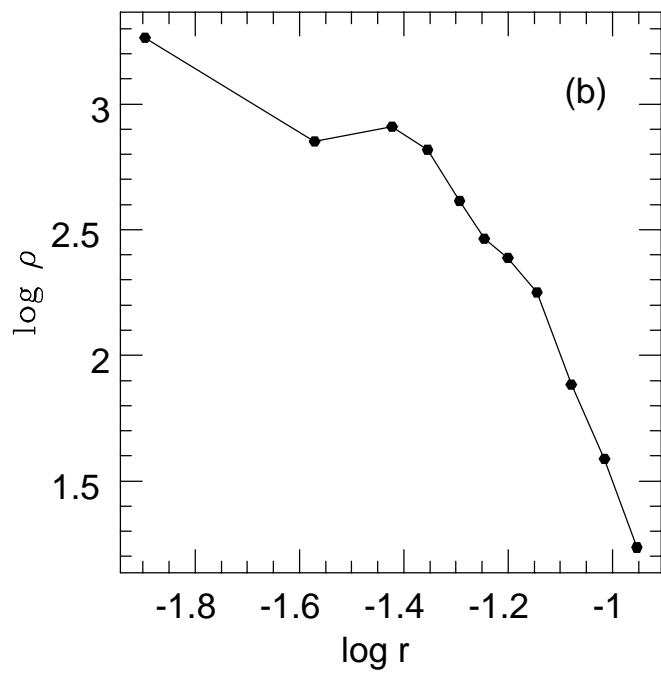
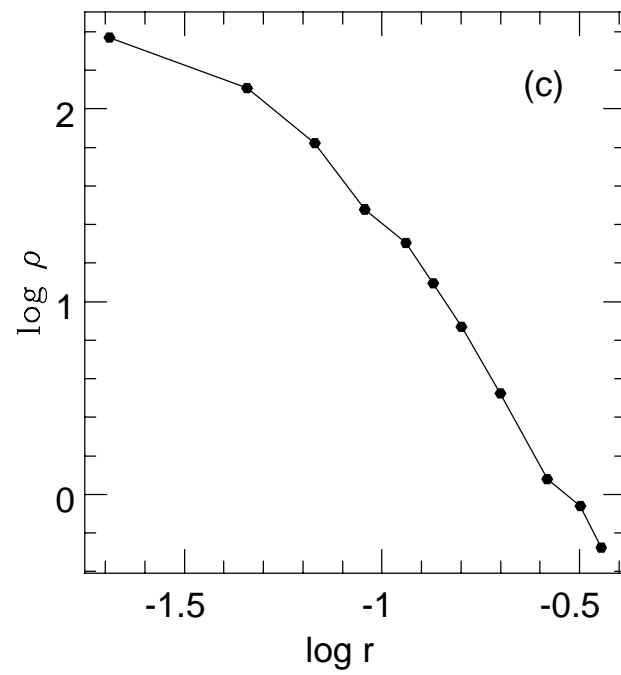
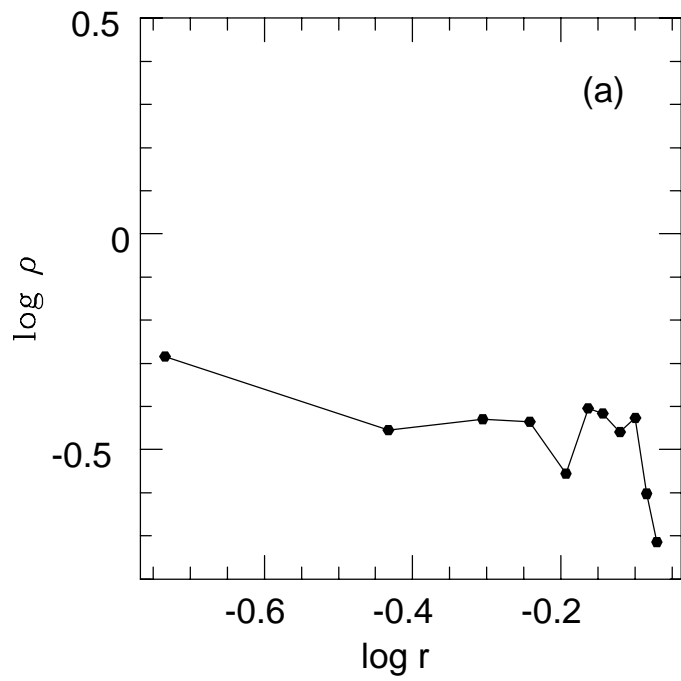
N	$\epsilon_{cut}(\text{N-body})/m_*\sigma^2$	$\epsilon_{cut}(\text{analytic})/m_*\sigma^2$
1000	34	34
2000	14	11.5
3000	9	9.9
5000	5	5.5

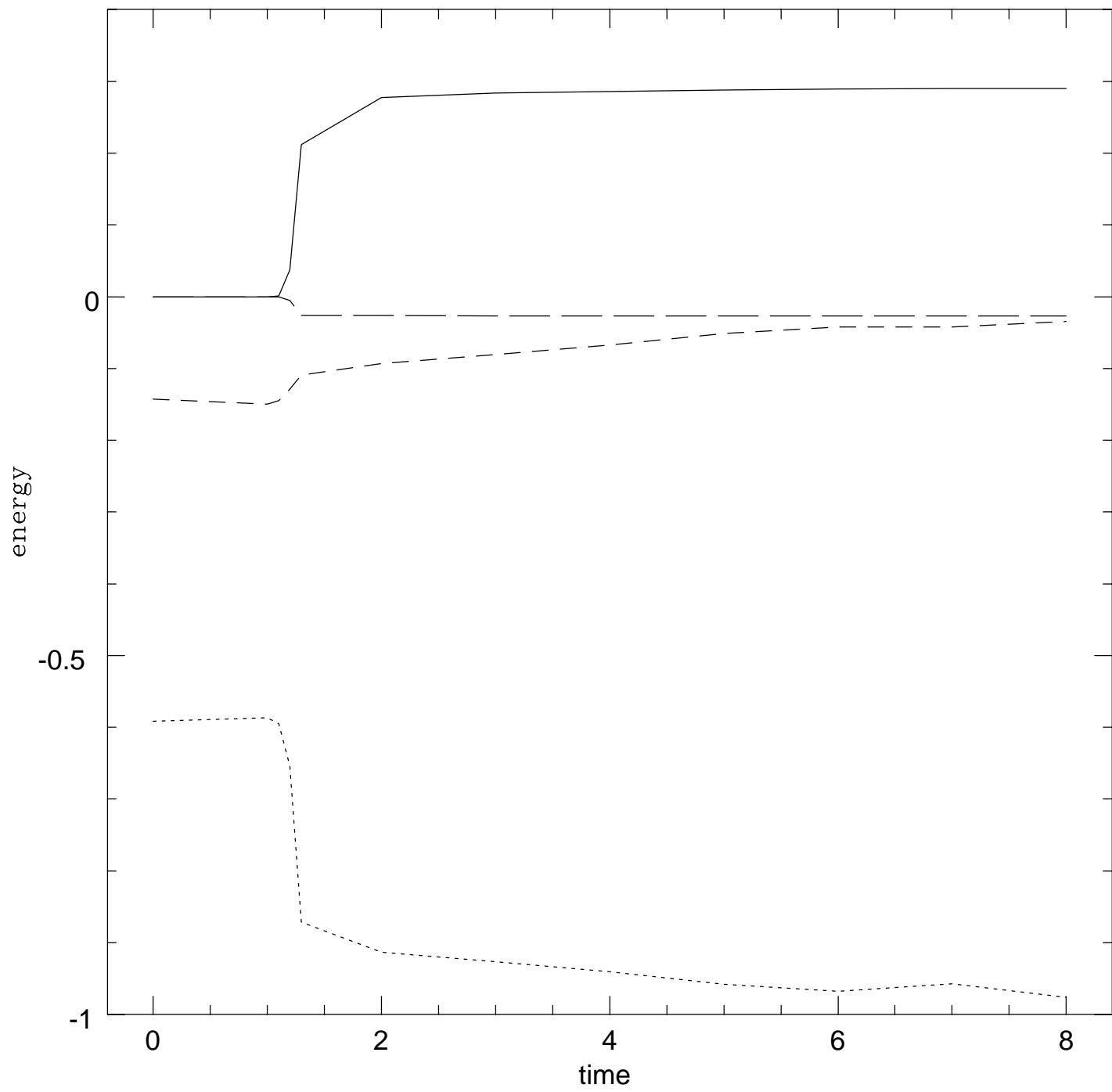
Table 6: A comparison of the cutoff energy observed in the N-body simulations and the analytic estimate.

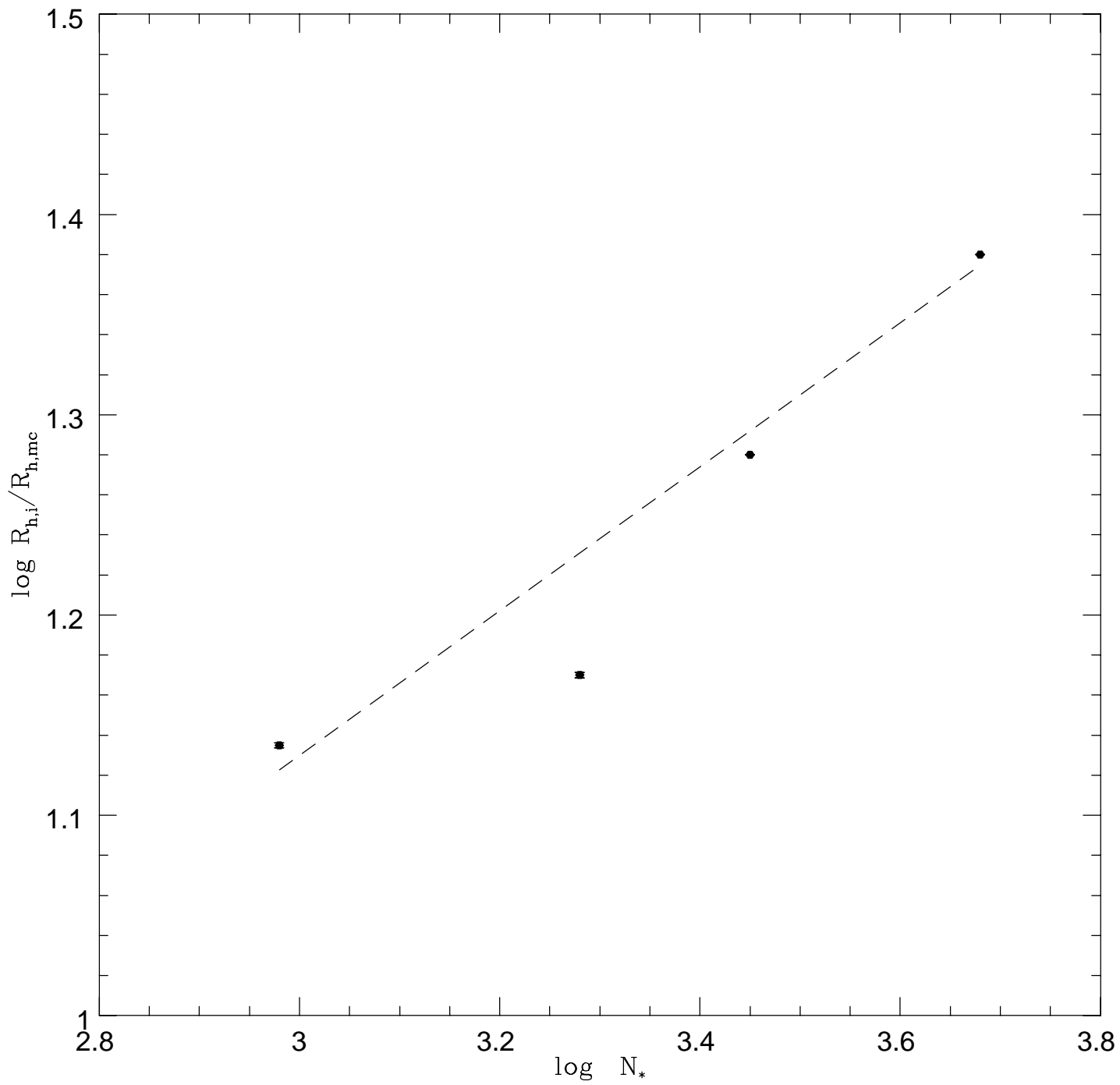
Table 7

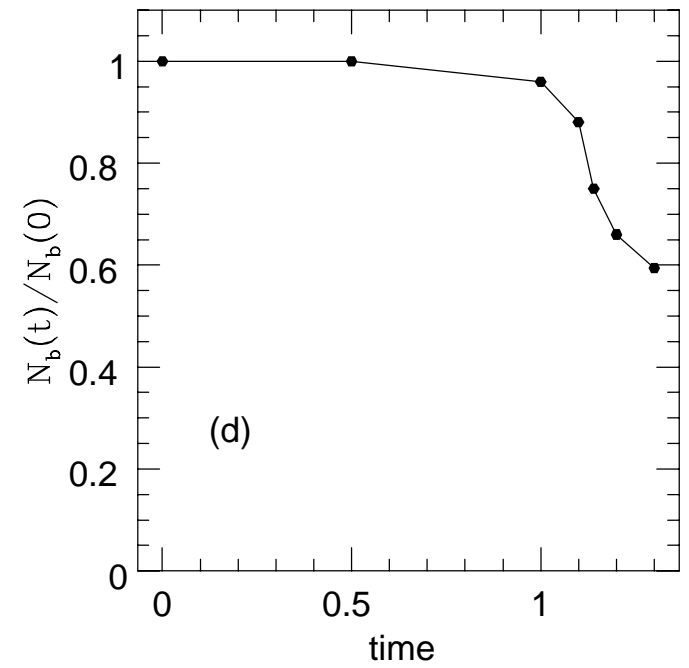
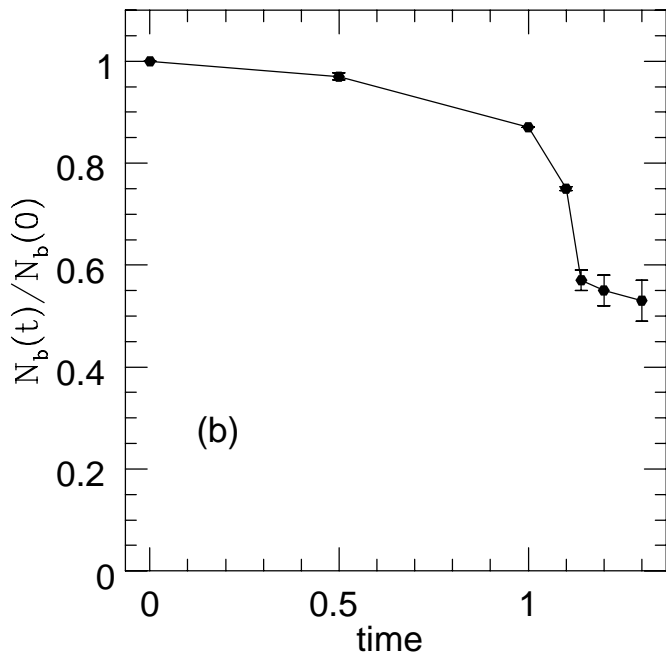
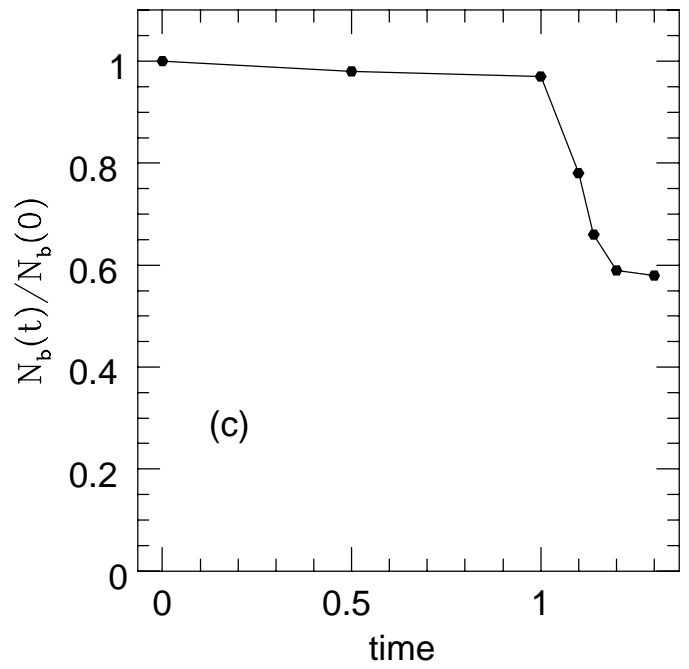
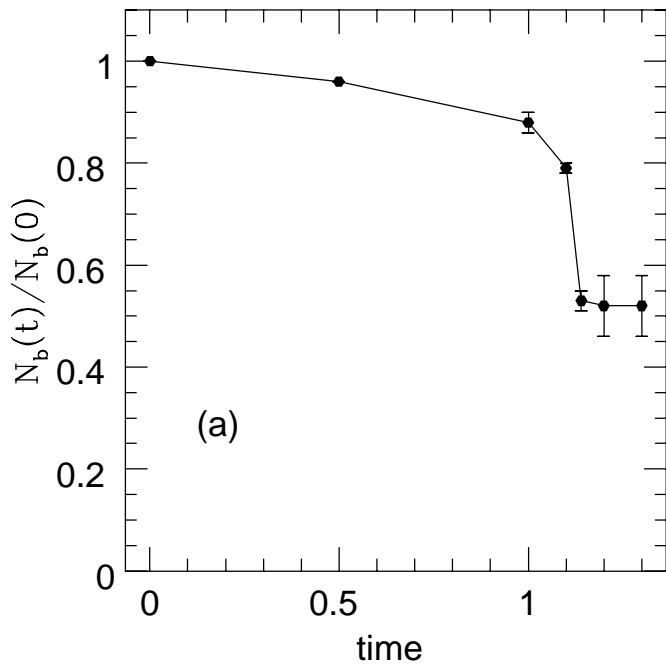
N	$D(\text{N-body})$	$D(\text{analytic})$
1000	0.48 ± 0.05	0.51
2000	0.48 ± 0.05	0.37
3000	0.42	0.39
5000	0.41	0.40

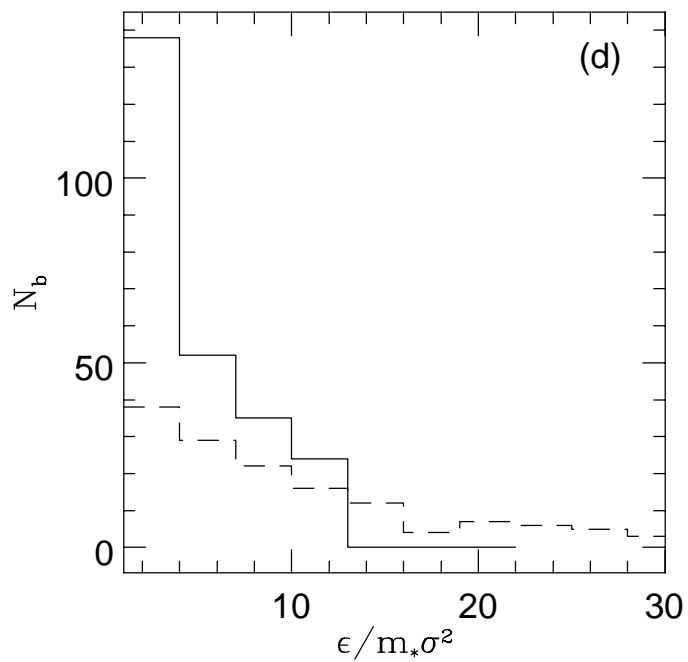
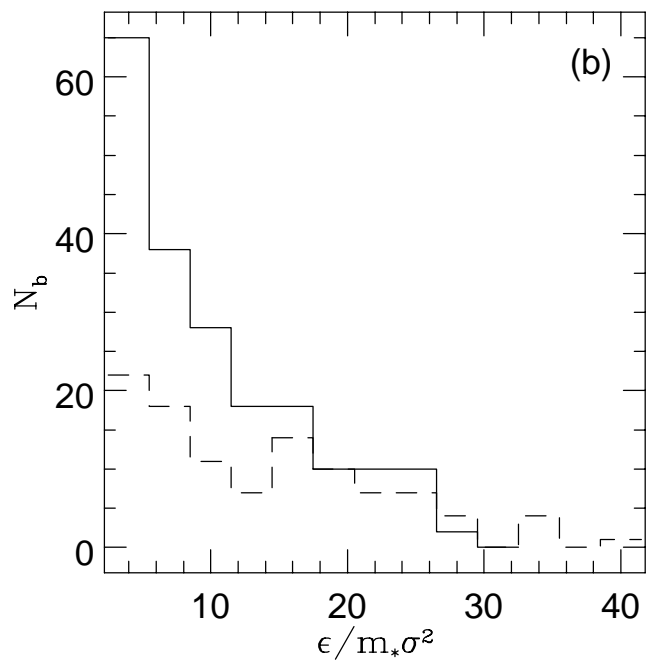
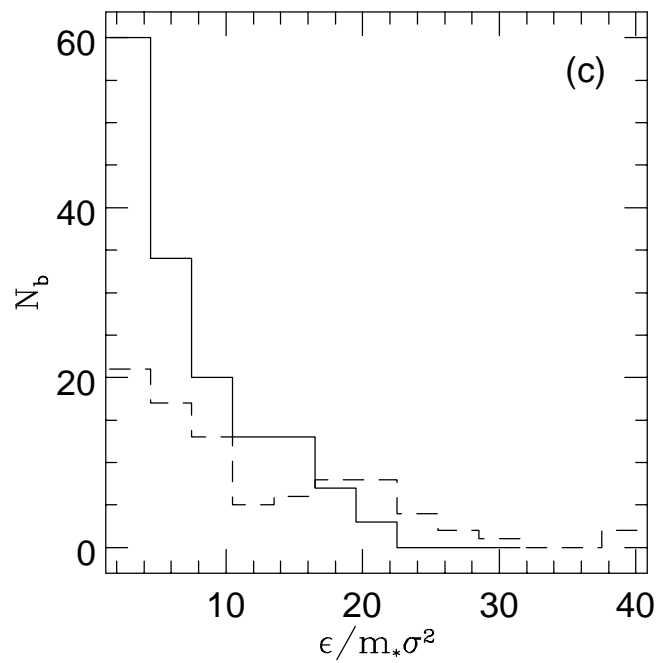
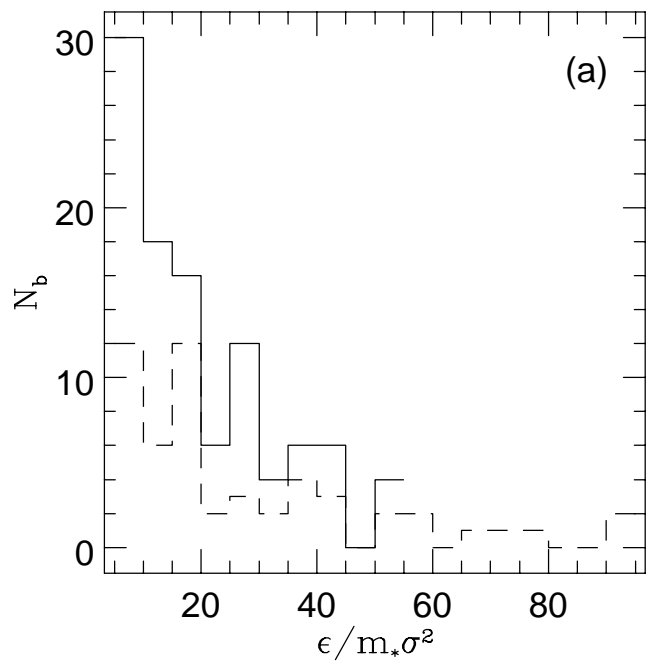
Table 7: A comparison of the fraction of disrupted binaries (D) in the N-body simulations and the analytic estimate.

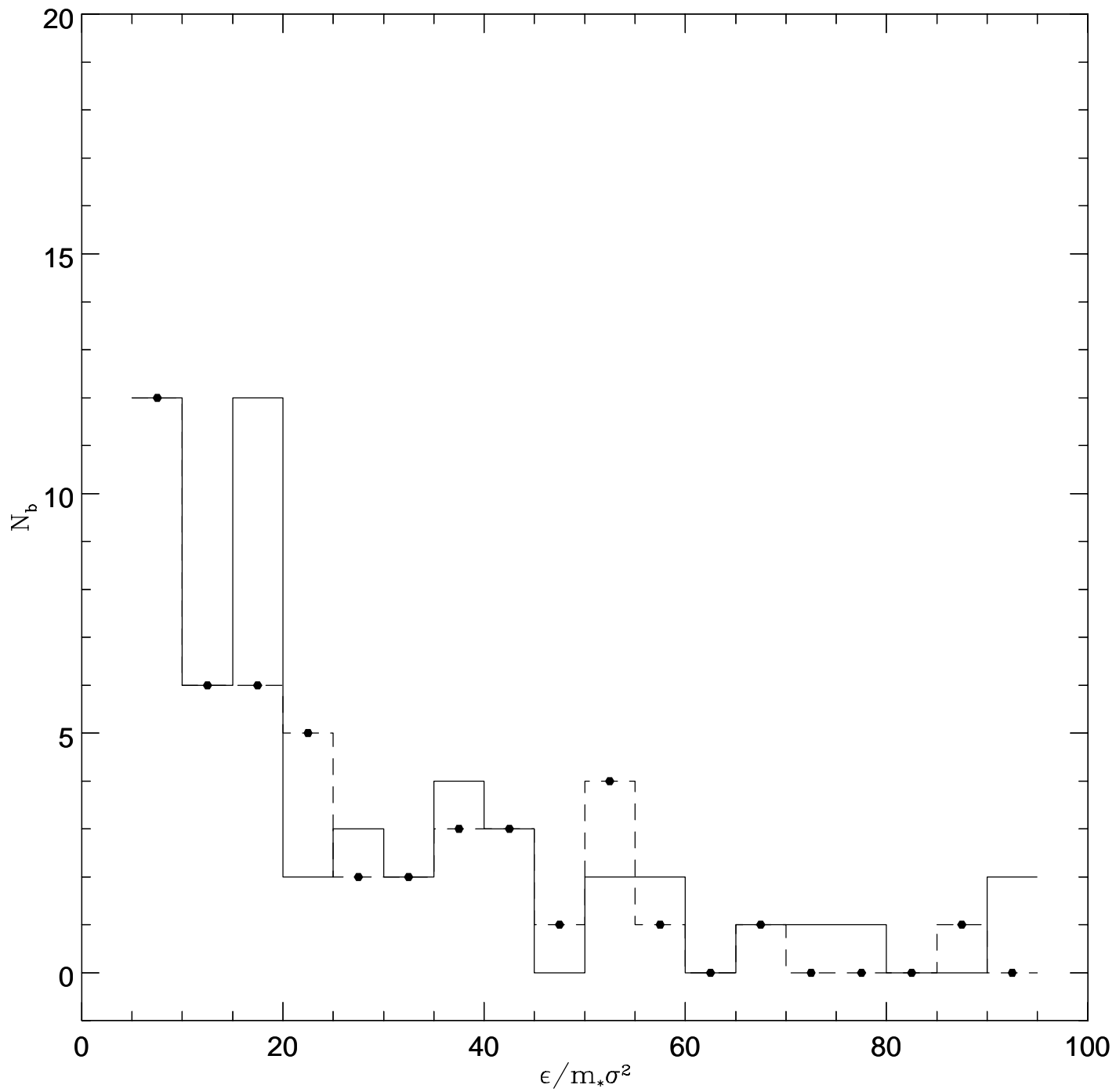


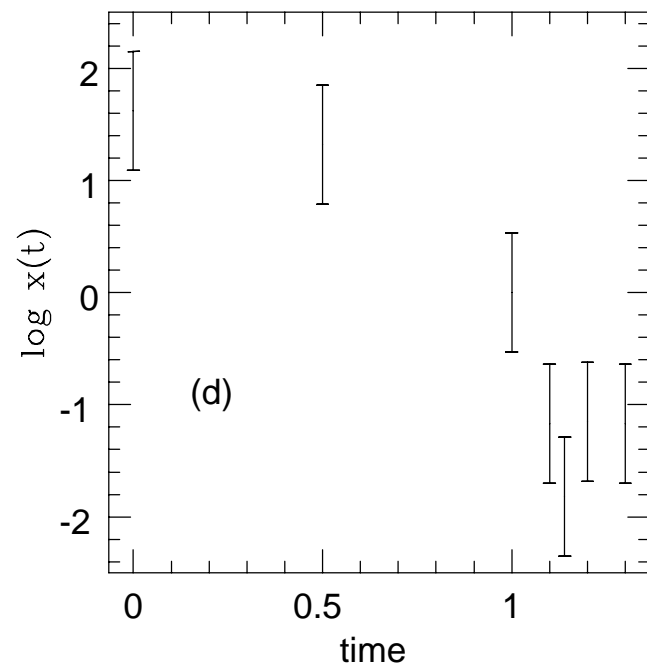
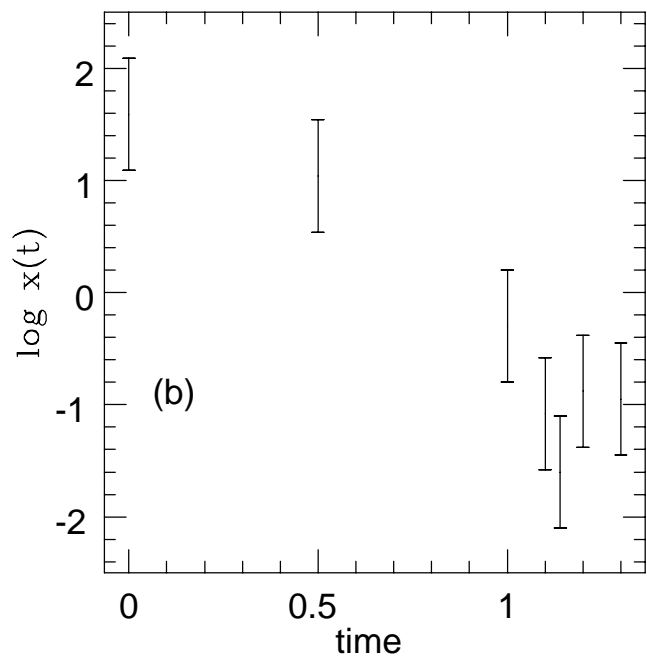
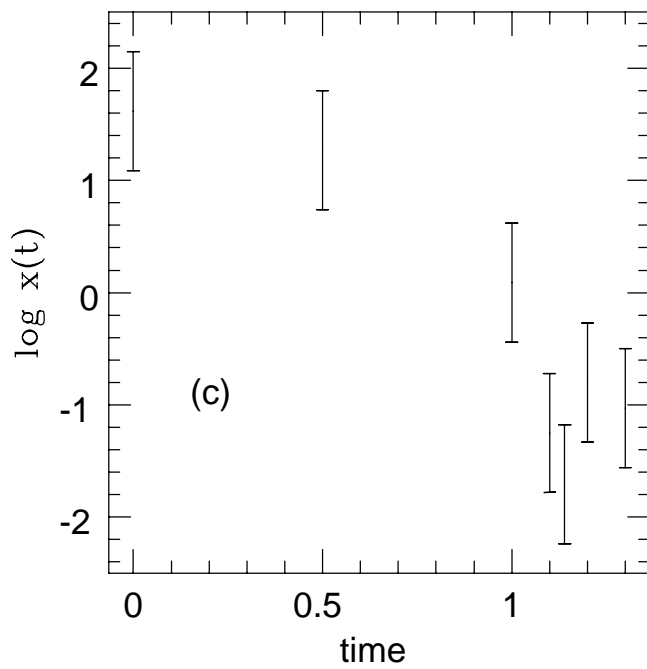
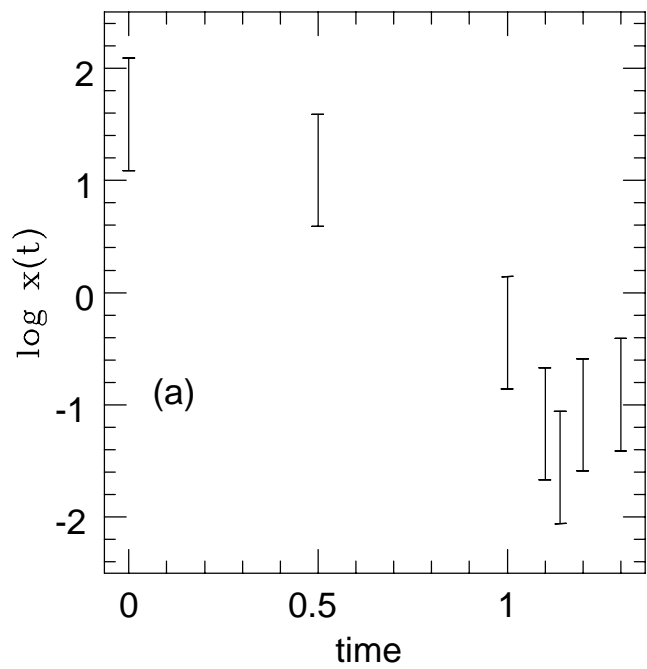


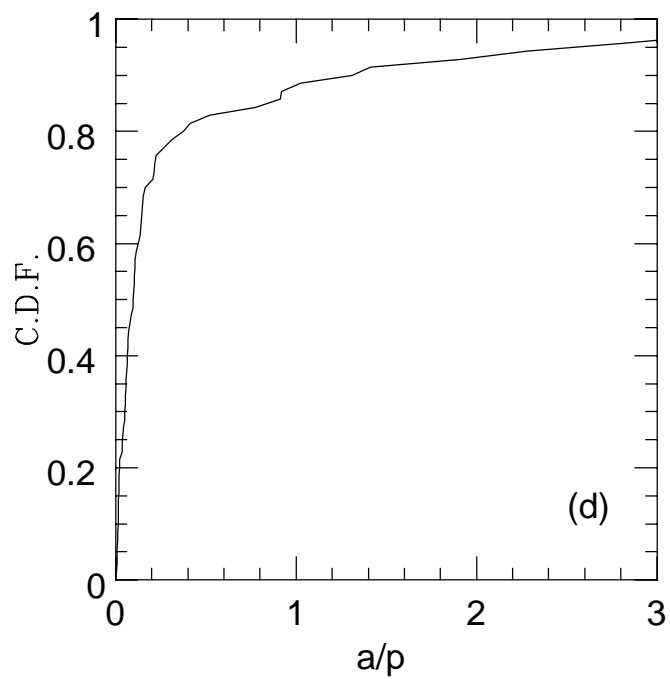
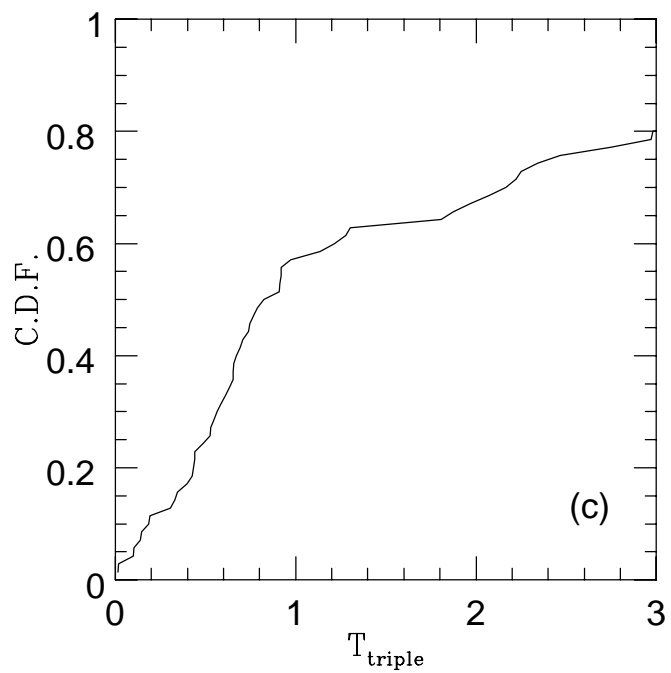
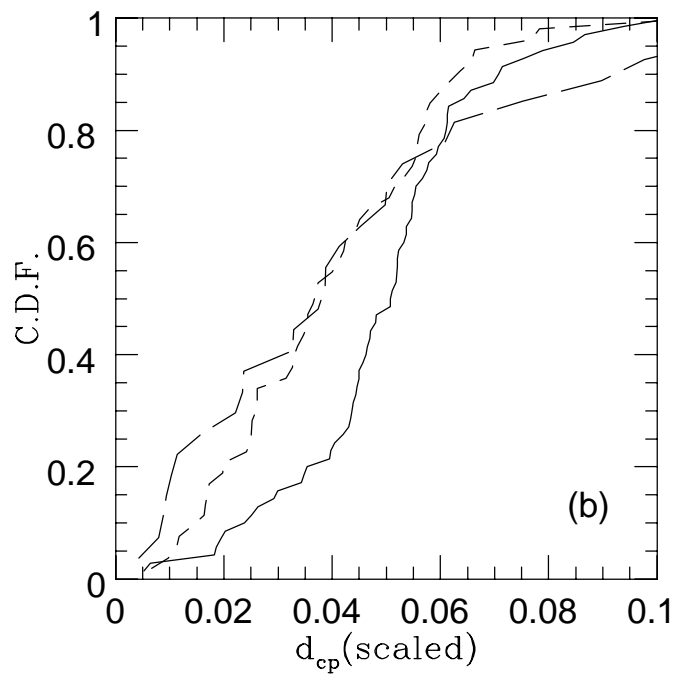
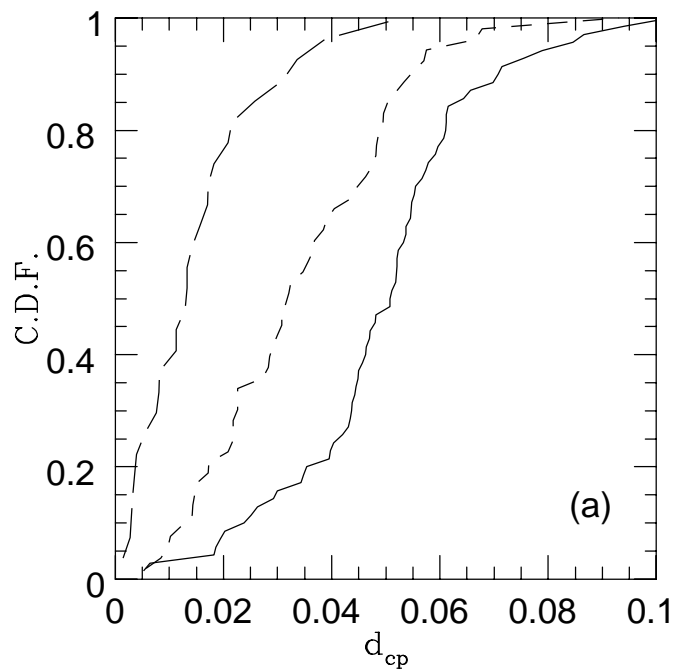


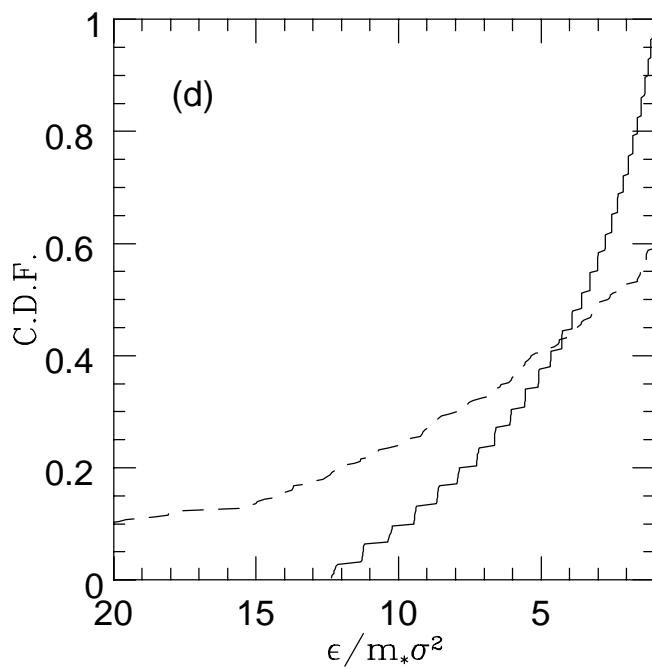
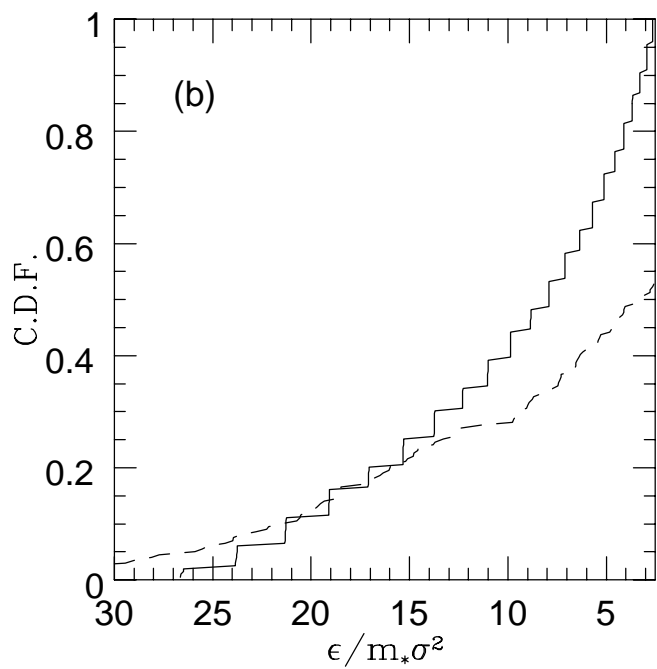
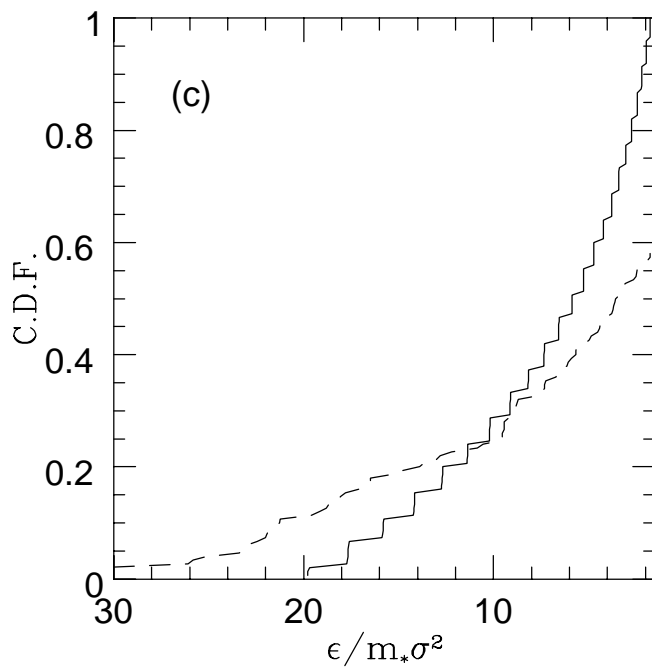
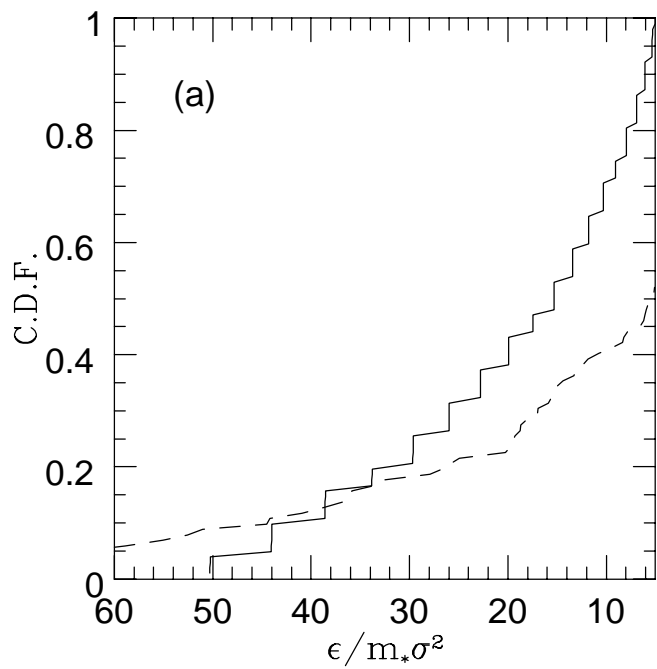


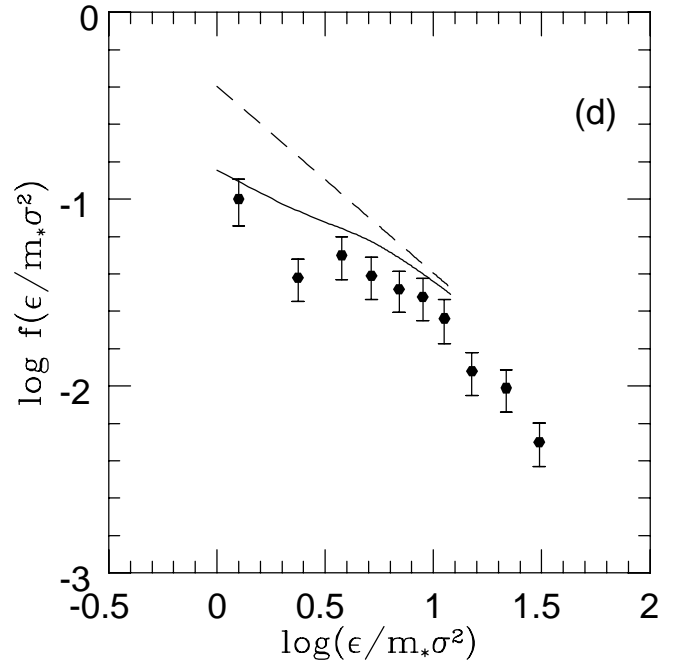
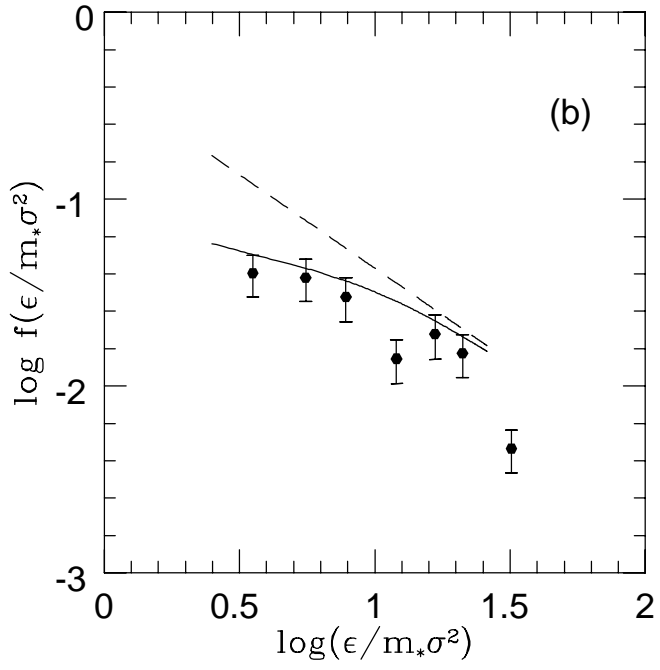
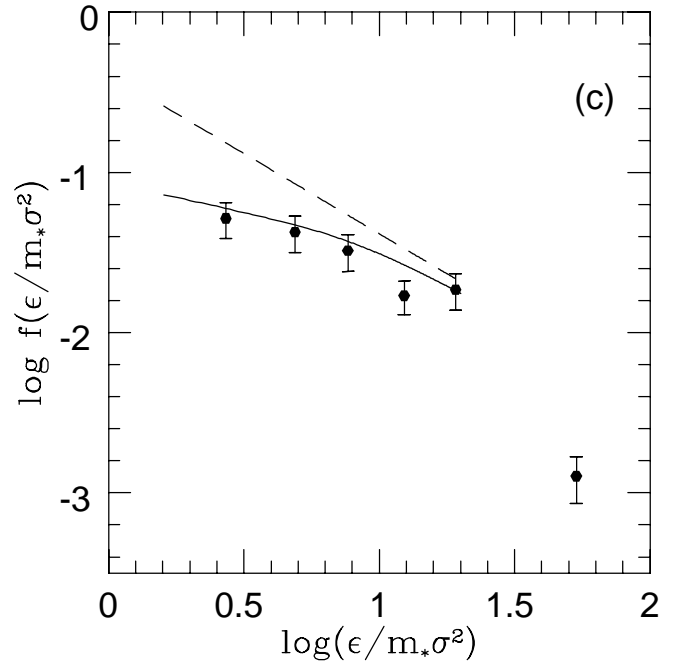
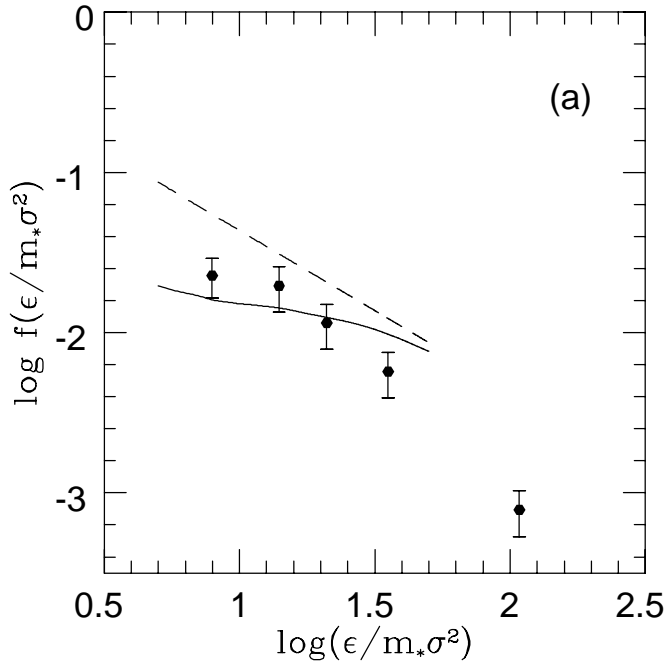


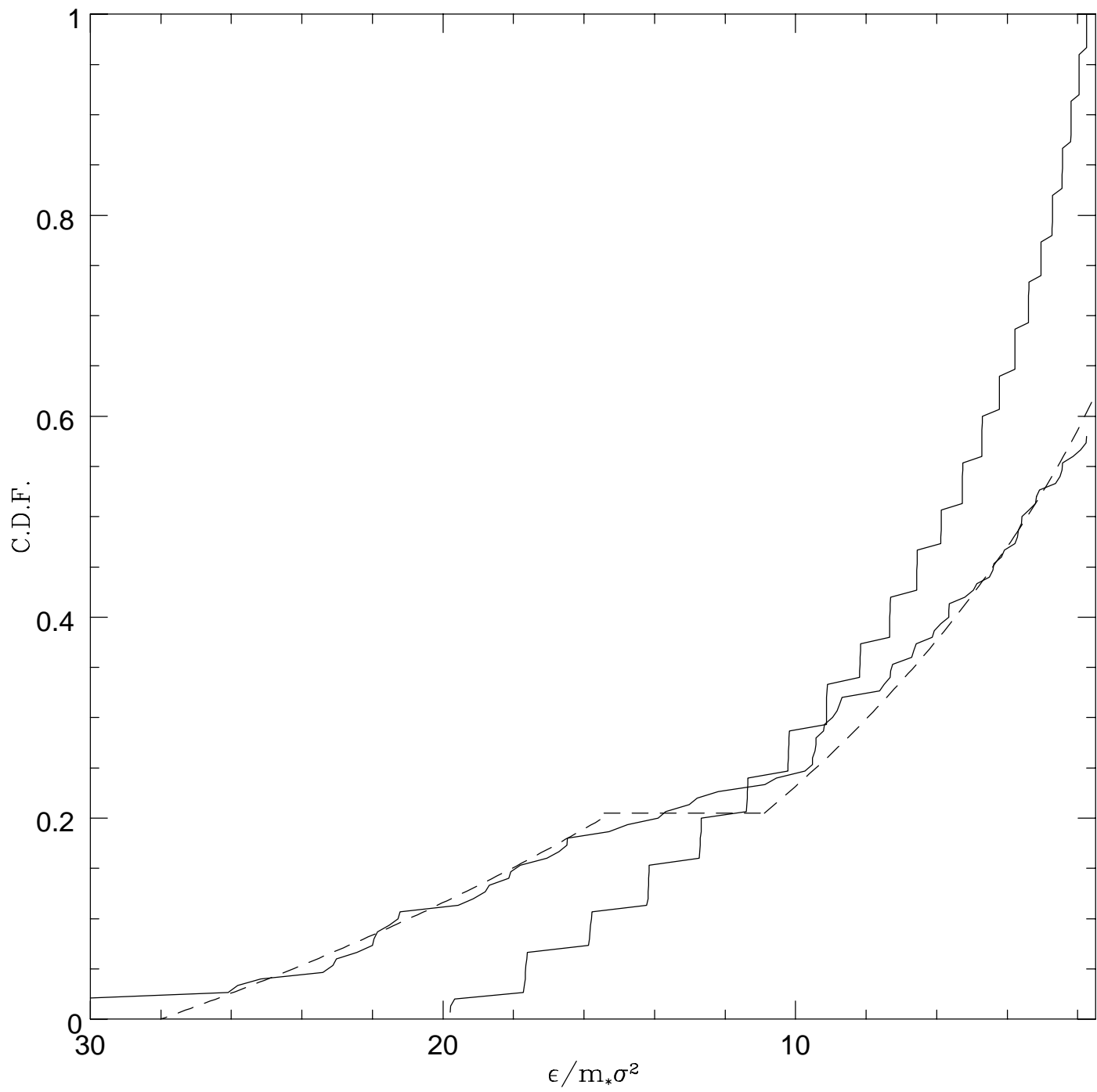












$P(r_M, \epsilon)$

$N = 1000$

